NISSUNA UMANA INVESTIGAZIONE SI PUO DIMANDARE VERA SCIENZIA
S'ESSA NON PASSA PER LE MATEMATICHE DIMOSTRAZIONI
LEONARDO DA VINCI

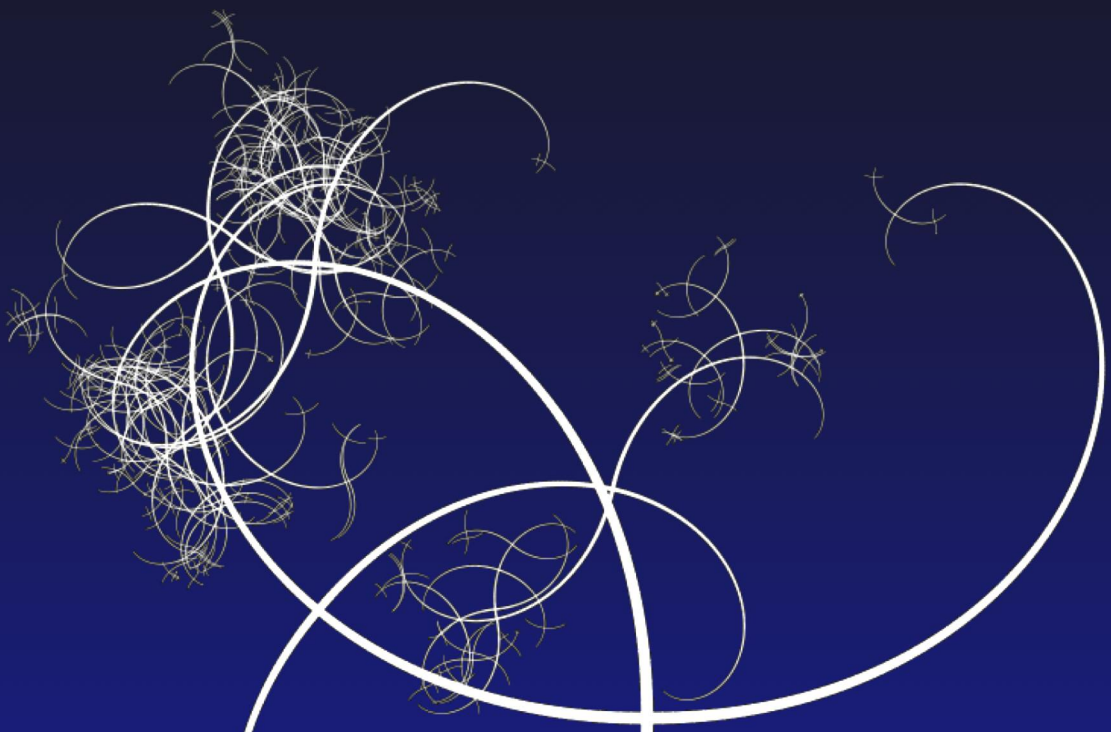

vol. 5 no. 2 2017

Mathematics and Mechanics *of* Complex Systems

Claude Boutin, Francesco dell'Isola,
Ivan Giorgio and Luca Placidi

LINEAR PANTOGRAPHIC SHEETS: ASYMPTOTIC MICRO-MACRO MODELS IDENTIFICATION

msp

MATHEMATICS AND MECHANICS OF COMPLEX SYSTEMS
Vol. 5, No. 2, 2017
dx.doi.org/10.2140/memocs.2017.5.127

LINEAR PANTOGRAPHIC SHEETS: ASYMPTOTIC MICRO-MACRO MODELS IDENTIFICATION

CLAUDE BOUTIN, FRANCESCO DELL'ISOLA,
IVAN GIORGIO AND LUCA PLACIDI

In this paper we consider linear pantographic sheets, which in their natural configuration are constituted by two orthogonal arrays of straight fibers interconnected by internal pivots. We introduce a continuous model by means of a micro-macro identification procedure based on the asymptotic homogenization method of discrete media. The rescaling of the mechanical properties and of the deformation measures is calibrated in order to comply with the specific kinematics imposed by the quasi-inextensibility of the fibers together with the large pantographic deformability. The obtained high-order continuum model shows interesting and exotic features related to its extreme anisotropy and also to the subcoercivity of its deformation energy. Some initial numerical simulations are presented, showing that the model can account for experimental uncommon phenomena occurring in pantographic sheets. The paper focuses on the precise analysis and the understanding of the effective behavior based on a well-calibration of the extension and bending phenomena arising at the local scale. In an upcoming work, the analysis will be extended to oblique arrays, some analytical solutions to proposed equations and some further applications.

1. Introduction

In the study of generalized (multiscale or architectured) continua, two different and complementary approaches can be identified:

(1) A phenomenological approach can be applied at the macroscopic scale: it gives a general framework and in general it is based on variational principles and methods [Mindlin 1965; Toupin 1964; Germain 1973; Gouin and Debieve 1986; Casal 1966; dell'Isola and Placidi 2011; dell'Isola et al. 2009; Lekszycki 1991]; however, using this approach it is not possible to make the influence of microstructure on macrophenomena become explicit. In other

Communicated by Pierre Seppecher.
MSC2010: 74KXX, 74QXX, 76AXX.
Keywords: pantographic structures, second gradient elasticity, woven fabrics.

words, a model is established, but the microstructured material to which it could be applied is unknown.

(2) Another approach involves a scale change, made possible through a homogenization. This method has been developed in vast literature (see, e.g., [Boutin and Auriault 1993; Pideri and Seppecher 1997; Bensoussan et al. 2011; Boutin and Soubestre 2011; Auriault et al. 2009; Allaire 1992; Alibert and Della Corte 2015; dell'Isola et al. 2016b; 2016c]) but has not been applied too often to the case of multiscale materials, in which a great contrast in physical properties appears at microlevel (see [Soubestre and Boutin 2012; Boutin et al. 2010]). Moreover, homogenization methods treat more particular cases and therefore they are not supposed to cover all situations. However, a careful homogenization technique gives the possibility of identifying the micromorphologies that lead to the macroscopic behavior characteristic of generalized continua.

Recently the attention has been attracted by a particular class of microstructure: that which produces so-called *pantographic continua* [dell'Isola et al. 2015b; 2016b; 2016c; 2016d; Giorgio et al. 2016; Madeo et al. 2015]. This kind of structure is inspired by several natural examples; indeed, some biological tissues present fibers that can be modeled in a similar way (see, e.g., [Melnik and Goriely 2013; Federico and Grillo 2012; Grillo et al. 2015] for some possible applications). Their interest was initially related to the possibility of proving the existence of purely second gradient continua [Alibert et al. 2003], but subsequently their practical applicability has been proven for woven fabrics and some "ad hoc" designed metamaterials (see, e.g., [Del Vescovo and Giorgio 2014; Bîrsan et al. 2012; Eremeyev and Lebedev 2011; Altenbach et al. 2011; dell'Isola et al. 2015b; Eremeyev 2016]). On the other hand, some interesting theoretical results were presented in [Chesnais et al. 2015; Boutin et al. 2010; Boutin and Soubestre 2011]. In these papers, some suitable homogenization methods were introduced to study the dynamics of periodic beam structures and other evidence was presented concerning the need to introduce second gradient continua when a high contrast of mechanical properties is present at microlevel.

In all considered cases, *directional* (anisotropic) materials with a high contrast in properties between shear and extension are studied. This paper, different to what was done in [Rahali et al. 2015], considers the case of extensible fibers and gives a more solid foundation to and generalizes the heuristic results presented in [Placidi et al. 2017] based on an accurate analysis of the different and relative order of magnitude of the involved physical phenomena.

In this paper we will use a micro-macro asymptotic identification method and obtain the macroscopic equilibrium equations for pantographic lattices in the neighborhood of a reference configuration. The analysis of the obtained equation is

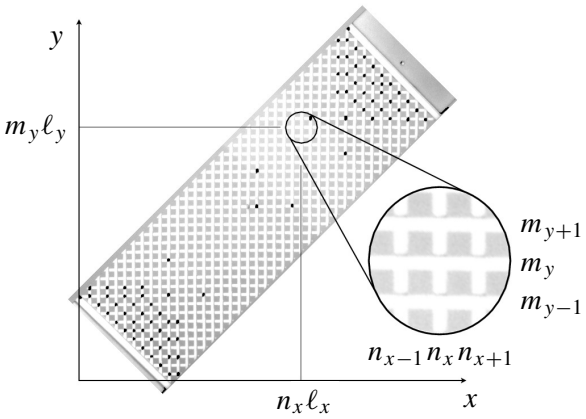

Figure 1. Topology of the pantographic lattice. The pivots are equally distributed on the whole sheet. The black points are indicating specific monitoring points during bias test experiments.

started and some equilibrium problems are solved by means of numerical simulations.

In a forthcoming paper we treat the generalized case of reference configurations constituted by two oblique arrays of straight beams, some semianalytical solutions and some further application.

2. Hypotheses and notations

Let us consider a periodic pantograph network of fibers (which we also call a pantographic lattice or pantographic sheet) formed of two families of continuous fibers arranged perpendicularly and along the axes x and y. The fibers oriented along x are identical, as well as those oriented along y. However, the two families may differ from one another. These fibers are connected by perfect pivots, with an axis perpendicular to the $\{x, y\}$ plane. The fibers oriented along x are spaced periodically by the length ℓ_y. Those oriented along y are spaced by ℓ_x. This defines the rectangular mesh, which is constituted by those two elements that are the portions of the orthogonal fibers that cross a pivot. Each pivot is referenced by two integers n_x and m_y, which are simply its discrete coordinates along the axes x and y, respectively. We will model each segment of fiber between two consequent nodes as a beam. The four beam elements connected to the pivot $\{n_x, m_y\}$ are denoted by $[n_x - 1, n_x]$ and $[n_x, n_x + 1]$ for the two elements oriented along x, or by $[m_y - 1, m_y]$ and $[m_y, m_y + 1]$ for the two elements oriented along y. The understanding of the reader is helped by Figure 1.

The parameters of the beam elements are their Young's modulus E_j, the area A_j of their sections and the moments of inertia I_j of their sections, where $j = x, y$.

The dimensions of the sections $\sqrt{A_j}$ are assumed small with respect to the lengths ℓ_j. Accordingly, the behavior of the interpivot elements can be effectively modeled by the Euler beam model. It is further assumed that the geometrical and the mechanical parameters of both types of beams are of the same order of magnitude: to be more precise, the period is characterized by the length $\ell = \sqrt{\ell_x \ell_y}$ in such a way that $O(\ell_x) = O(\ell_y) = \ell$. We also introduce the following dimensionless quantities: $\ell_x^\star = \ell_x/\ell$ and $\ell_y^\star = \ell_y/\ell$ so that $\ell_x^\star \ell_y^\star = 1$ and $O(\ell_x^\star) = O(\ell_y^\star) = O(1)$.

Note that the specificity of the adopted assumption of beam behavior is that the length of the arrays is not considered (i.e., the fibers are not treated as beams) but instead, this is the topology of the pantographic lattice that leads to a local beam description.

We study in the $\{x, y\}$ plane the quasistatic small deformations of the lattice in the neighborhood of its initial equilibrium position where the lattice is periodic and has a rectangular period. It is also assumed that the spatial variations of the deformation and placement fields occur at large-scale and have a characteristic variation length L that is large compared to the size of period ℓ; in other words, to have a relevant variation of the deformation fields, the space variables must have a large increment relative to ℓ.

These considerations naturally introduce the small parameter to be used for specifying scale separation:

$$\varepsilon = \ell/L \ll 1.$$

The macroscopic description of the system, valid at the dominant order, is reached for $\varepsilon \to 0$.

3. Homogenization method: multiscale asymptotic heuristic approach

Let us construct the global behavior from the local behavior of beam elements connected by pivots. To do this, the problem is first discretized exactly and then it is converted into a continuum macroscopic formulation by an asymptotic homogenization procedure.

Using the balance laws of an Euler beam, the contact actions (normal and shear forces and moments) at the ends of each beam element are explicitly expressed in terms of the kinematic variables (displacements and rotations) evaluated at the same ends. The balance of each element is thereby assured. We will consider the cases in which the beam elements between the nodes deform in a quasistatic regime. In other words, our treatment will be applicable when, in considered phenomena, there is a (quasi-)instantaneous equilibrium, at the level of the periodic cell, of the interconnected beams. Sometimes this assumption is referred to as the *assumption of local microscopic instantaneous equilibrium*. This approach is relevant when dealing with phenomena of slow-time evolution.

As a consequence of the exact discretization, to specify the conditions of the global equilibrium conditions, it is necessary and sufficient to focus on the equilibrium of each one of the pivots, which will play the role of material points of the homogenized continuum. It is therefore expressed, in each pivot, the balance of forces and moments applied by the four elements therein connected (belonging to the two orthogonal fibers that intersect at each pivot). This gives an *exact* representation of the original problem in a discrete form of finite difference type, with the variables being the kinematic variables and the actions of each element, evaluated at the pivot-locations. One has to explicitly remark that in the set of the aforementioned four elements, one can distinguish two pairs (parallel in the reference configuration) which are indeed part of the same fiber: moving from one to the other elements belonging to the same fiber, the displacements and rotations are continuous (see Figure 1, x-fiber and y-fiber).

Remark also that the action of a pivot on the two continuous fibers which the pivot itself is interconnecting is modeled here as concentrated (in a point) force and couple; of course, by the action and reaction principle, the action of the pivot on the fiber of one array is opposite to the action exerted by the same pivot on the fiber of the other array.

The passage from the exact discrete formulation to the macroscopic continuous description, valid at the dominant order, is performed as follows [Caillerie 1984]. We assume that the overall behavior of the system can be described by a set of macroscopic fields, the generic element of which is denoted by $Q(x, y)$.

Discrete variables $q_{(n_x,m_y)}$ at the pivots are considered as the values at these points of continuous functions $Q(x, y)$.

This procedure has been described in general already in the works by Piola [2014] (he seems to us to be among the first scientists having introduced such a heuristic method of homogenization; see [dell'Isola et al. 2016d; Rahali et al. 2015]); however, he applied it specifically only to the case of fluids.

We therefore set

$$q_{(n_x,n_y)} = Q(x_n, y_m), \quad x_n = n_x \ell_x, \quad y_m = m_y \ell_y.$$

Consistent with the hypothesis of separation of scale, these continuous functions vary at large scales, such as $O(L)$. Consequently, the increments of the interpivot distance $O(\ell)$ can be expressed by the Taylor expansions of macroscopic fields. Thus, the finite difference of the discrete formulation is converted into series by introducing successive gradients of the macroscopic functions. As the distances between the pivots are constant due to the periodicity, the terms of such series are of the type, for example, $\ell_x^k \partial^k Q/\partial x^k = O(\ell_x^k/L^k) O(Q) = \varepsilon^k O(Q)$, with a multiplication factor. They therefore involve the orders of magnitude in powers of ε. As we are interested in situations where $\varepsilon \to 0$, we need the following specification for

the consistency of the orders of magnitude, i.e., we need to represent the functions $Q(x, y)$ in the form of asymptotic expansions of the type:

$$Q(x, y) = \sum_{k=0}^{\infty} \varepsilon^k Q^{(k)}(x, y), \quad O(Q^{(k)}) = O(Q^{(0)}).$$

These asymptotic expansions are to be used in the equations of equilibrium expressed via Taylor expansions. The dimensionless parameters that emerge from this formulation must be weighted in powers of ε to translate correctly the dominant mechanisms in the studied system [Boutin and Hans 2003; Hans and Boutin 2008]. This normalization of the balance equations preserves the *same* local physics during the transition to the limit $\varepsilon \to 0$. Consequently, the macroscopic model in the limit preserves — at the dominant order — the same local physics than that prevailing in the real system, where the scale ratio ℓ/L takes small but finite values.

After the aforementioned normalization, we obtain a series of equilibrium conditions in terms of the powers of ε, which may be solved term by term. The macroscopic description, at the dominant order, is constituted by the first nontrivial differential system on the macroscopic variables.

4. Micromodeling of pantographic lattices

In the literature, much attention has been paid to lattices of beams interconnected by clamping constraints and to trusses [Németh and Kocsis 2014; Liew et al. 2000; Noor et al. 1978]. However, the existence of so called "floppy modes" at the microlevel in the pantographic structures requires the most attentive consideration. To be more precise: what we call a floppy mode is a deformation of the microstructure to which is associated a vanishing energy (for more details, see [Alibert et al. 2003; Seppecher et al. 2011]). An intuitive consequence of the existence of floppy modes is that for the effective medium, the standard condition of coerciveness is not verified and therefore this concept needs to be modified or generalized. Actually one can decompose the space of deformations into a coercive subspace plus the space of floppy modes and the role of the boundary condition becomes more determinant in well-posed problems.

We used these microscopic floppy modes to prove that, in general, the class of first-gradient continua (those introduced by Cauchy and usually considered in continuum mechanics; see, e.g., [dell'Isola et al. 2016a; 2015c]) is not enough to describe, at a macrolevel, all conceivable physical systems. In particular, when there is high contrast (see [Camar-Eddine and Seppecher 2001; Pideri and Seppecher 1997; Hans and Boutin 2008; Boutin and Soubestre 2011; Cecchi and Rizzi 2001]) in physical properties at the microlevel, it may become necessary at the macrolevel to introduce higher-order continua (see [dell'Isola et al. 2012; 2016e]).

The analysis which we present adapts the studies presented in [Boutin et al. 2010; Boutin and Soubestre 2011; Hans and Boutin 2008; Soubestre and Boutin 2012] to the case of pantographic lattices to take into account their behavior, which can be regarded as being somehow exotic.

We start by using the framework of *local microscopic instantaneous equilibrium* to formulate a mesolevel model where the lattice is described as a set of nodes (the pivots) interconnected by beam element.

4.1. ***Characterization of the mechanical behavior of a beam element.*** Let the section of the considered straight (in the reference configuration) beam be A, its moment of inertia being I, and let the material constituting it be elastic, isotropic and with Young's modulus E. We denote (referring to the beam planar reference configuration) by v the axial displacement, by w the transverse displacement, by N the normal force, by T the shear force and by M the bending moment (we will be using the French convention for the orientation of axes). These contact actions are defined as that of the part $s < 0$ on part $s > 0$, where s designates the abscissa along the axis of the beam. Consider a portion of the beam between two points B and C, spaced apart by a distance ℓ that is large enough compared to the size $\sqrt{A}$ of the beam section. The Euler beam theory can therefore be used. Accordingly, the rotation of the section is related to the transverse displacement via the relation $\theta(s) = \mathrm{d}w(s)/\mathrm{d}s$. The constitutive equations of the beam are the following:

$$N(s) = EA\frac{\mathrm{d}v}{\mathrm{d}s}, \quad M(s) = -EI\frac{\mathrm{d}^2 w}{\mathrm{d}s^2}, \tag{1}$$

and, in the quasistatic regime, the equilibrium equations in differential form are expressed by

$$\frac{\mathrm{d}N}{\mathrm{d}s} = 0, \quad \frac{\mathrm{d}T}{\mathrm{d}s} = 0, \quad \frac{\mathrm{d}M}{\mathrm{d}s} + T = 0. \tag{2}$$

Suppose that for the point B (and C), the displacements and the rotation are v^B, w^B and θ^B (respectively v^C, w^C and θ^C). The forces and moment at B and at C are determined using the equations of beams. They are expressed as a function of the kinematic variables as follows:

$$N^B = N^C = \frac{EA}{\ell}(v^B - v^C), \tag{3}$$

$$T^B = T^C = \frac{12EI}{\ell^3}\big(w^B - w^C + \tfrac{1}{2}\ell(\theta^B + \theta^C)\big), \tag{4}$$

$$M^B = \frac{6EI}{\ell^2}\big(w^B - w^C + \tfrac{1}{3}\ell(2\theta^B + \theta^C)\big), \tag{5}$$

$$M^C = -\frac{6EI}{\ell^2}\big(w^B - w^C + \tfrac{1}{3}\ell(\theta^B + 2\theta^C)\big). \tag{6}$$

Expressions of N involve the axial EA/ℓ rigidities, while T and M involve bending $12EI/\ell^3$ rigidities. The beam's slenderness hypothesis $\sqrt{A} \ll \ell$ implies that such rigidities differ significantly. In fact, considering beams of regular section (for instance, the rectangular section of length's sides a and b, with $b = O(a) = O(\sqrt{A})$), then $A = ab$, $I = ba^3/12$ and $12I/A = a^2 = O(A)$, and consequently the rigidity ratio R is

$$R = \frac{12EI}{\ell^3}\frac{\ell}{EA} = \frac{12I}{\ell^2 A} = O\left(\frac{A}{\ell^2}\right) \ll 1. \tag{7}$$

This strong stiffness contrast plays an essential role in the functioning of the system. Hereafter we take into account explicitly that the aspect ratio of the elements is $\sqrt{A}/\ell = O(\varepsilon)$ which leads to

$$R = \frac{12EI}{\ell^3}\frac{\ell}{EA} = O(\varepsilon^2). \tag{8}$$

4.2. ***Discrete kinematic variables and equilibrium at pivots.*** Because of the operating principle of an internal pivot, the ends of the four elements connected to it undergo the same displacement u_x (u_y) along the axis x (y), but rotations of those elements belonging to fibers with distinct orientations are not identical; the coinciding ends of the two elements oriented along x (y) undergo the same rotation θ_x (θ_y). Thus, each pivot $\{n_x, m_y\}$ is described by four kinematic variables $u_{x(n_x,m_y)}$, $u_{y(n_x,m_y)}$, $\theta_{x(n_x,m_y)}$ and $\theta_{y(n_x,m_y)}$.

The equilibrium at a pivot results:

(i) in the balances of force (exerted on the pivot) along x and y, and

(ii) in the continuity of both moment fields arising in the beam elements oriented either along x or along y.

These four equations expressed at the pivot $\{n_x, m_y\}$ take the following forms:

- balance of force along x:

$$-T^C_{[m_y-1,m_y]} + T^B_{[m_y,m_y+1]} + N^C_{[n_x-1,n_x]} - N^B_{[n_x,n_x+1]} = 0, \tag{9}$$

- balance of force along y:

$$T^C_{[n_x-1,n_x]} - T^B_{[n_x,n_x+1]} + N^C_{[m_y-1,m_y]} - N^B_{[m_y,m_y+1]} = 0, \tag{10}$$

- balance of moments for the elements along x:

$$M^C_{[n_x-1,n_x]} - M^B_{[n_x,n_x+1]} = 0, \tag{11}$$

- balance of moments for the elements along y:

$$M^C_{[m_y-1,m_y]} - M^B_{[m_y,m_y+1]} = 0. \tag{12}$$

Here, we have denoted by the symbol $Q^D_{[p,q]}$ the value of the field Q at the extremity $D = C$ or $D = B$ of the beam element connecting the node p and the node q, where p and q are consecutive in either the x or y direction.

The component u_x (u_y) of the pivot displacement is:

(i) the axial displacement of the ends of the beam element oriented along x (y), and

(ii) the opposite transverse (direct) displacement of the ends of the beam element along y (along x). The change of sign results from different orientations of the global frame and of the local frame of the y-oriented fibers.

Thus, by substituting in (9)–(12) the forces by their expressions in terms of the displacement fields (3)–(6), the balance of force along x is obtained as

$$\frac{12E_yI_y}{\ell_y^3}\big((u_{x(n_x,m_y-1)} - 2u_{x(n_x,m_y)} + u_{x(n_x,m_y+1)}) + \tfrac{1}{2}\ell_y(-\theta_{y(n_x,m_y-1)} + \theta_{y(n_x,m_y+1)})\big) + \frac{E_xA_x}{\ell_x}(u_{x(n_x-1,m_y)} - 2u_{x(n_x,m_y)} + u_{x(n_x+1,m_y)}) = 0. \quad (13)$$

The continuity at the nodes of bending moments of the elements oriented along y (after the simplification by $2E_yI_y/\ell_y$) reads

$$\frac{3}{\ell_y}(u_{x(n_x,m_y-1)} - u_{x(n_x,m_y+1)}) - (\theta_{y(n_x,m_y-1)} + 4\theta_{y(n_x,m_y)} + \theta_{y(n_x,m_y+1)}) = 0, \quad (14)$$

the balance of force along y reads

$$\frac{12E_xI_x}{\ell_x^3}\big((u_{y(n_x-1,m_y)} - 2u_{y(n_x,m_y)} + u_{y(n_x+1,m_y)}) + \tfrac{1}{2}\ell_x(-\theta_{x(n_x-1,m_y)} + \theta_{x(n_x+1,m_y)})\big) + \frac{E_yA_y}{\ell_y}\big(u_{y(n_x,m_y-1)} - 2u_{y(n_x,m_y)} + u_{y(n_x,m_y+1)}\big) = 0, \quad (15)$$

and finally the continuity at the nodes of bending moments of the elements oriented along x (after the simplification by $2E_xI_x/\ell_x$) reads

$$\frac{3}{\ell_x}(-u_{y(n_x-1,m_y)} + u_{y(n_x+1,m_y)}) - (\theta_{x(n_x-1,m_y)} + 4\theta_{x(n_x,m_y)} + \theta_{x(n_x+1,m_y)}) = 0. \quad (16)$$

These four equations are split into two independent groups of equations: (13)–(14) couples the variables u_x and θ_y; while (15)–(16) couples the variables u_y and θ_x. Thus, it is sufficient to treat (13)–(14), being that the results of (15)–(16) are easily deduced by changing the roles of axes x and y.

4.3. ***Continuous formulation and asymptotic expansions.*** Let us introduce continuous kinematic descriptors (denoted by uppercase letters) coinciding with the discrete kinematic variables of the pivots $\{n_x, m_y\}$ with coordinates $x_n = n\ell_x$ and $y_m = m\ell_y$:

$$u_{x(n_x,m_y)} = U_x(x_n, y_m), \quad \theta_{y(n_x,m_y)} = \Theta_y(x_n, y_m), \tag{17}$$

$$u_{y(n_x,m_y)} = U_y(x_n, y_m), \quad \theta_{x(n_x,m_y)} = \Theta_x(x_n, y_m), \tag{18}$$

and use Taylor series expansions to express the terms of the finite difference equations (13)–(14). By introducing the dimensionless variables $x^\star = x/L$ and $y^\star = y/L$, we have (for comparison, see [Piola 2014; Carcaterra et al. 2015])

$$\begin{aligned} &u_{x(n_x,m_y-1)} - 2u_{x(n_x,m_y)} + u_{x(n_x,m_y+1)} \\ &\qquad = \ell_y^2 \frac{\partial^2 U_x}{\partial y^2}(x_n, y_m) + \frac{2}{4!}\ell_y^4 \frac{\partial^4 U_x}{\partial y^4}(x_n, y_m) + O\left(\ell_y^6 \frac{\partial^6 U_y}{\partial y^6}\right) \\ &\qquad = \varepsilon^2 \ell_y^{\star 2} \frac{\partial^2 U_x}{\partial y^{\star 2}} + \varepsilon^4 \ell_y^{\star 4} \frac{2}{4!} \frac{\partial^4 U_x}{\partial y^{\star 4}} + \varepsilon^6 \ell_y^{\star 6} \frac{2}{6!} \frac{\partial^6 U_x}{\partial y^{\star 6}} + O(\varepsilon^8), \end{aligned} \tag{19}$$

$$\begin{aligned} &u_{x(n_x-1,m_y)} - 2u_{x(n_x,m_y)} + u_{x(n_x+1,m_y)} \\ &\qquad = \varepsilon^2 \ell_x^{\star 2} \frac{\partial^2 U_x}{\partial x^{\star 2}} + \varepsilon^4 \ell_x^{\star 4} \frac{2}{4!} \frac{\partial^4 U_x}{\partial x^{\star 4}} + \varepsilon^6 \ell_x^{\star 6} \frac{2}{6!} \frac{\partial^6 U_x}{\partial x^{\star 6}} + O(\varepsilon^8), \end{aligned} \tag{20}$$

similarly,

$$\begin{aligned} &-\theta_{y(n_x,m_y-1)} + \theta_{y(n_x,m_y+1)} \\ &\qquad = 2\varepsilon \ell_y^\star \frac{\partial \Theta_y}{\partial y^\star} + \varepsilon^3 \ell_y^{\star 3} \frac{2}{3!} \frac{\partial^3 \Theta_y}{\partial y^{\star 3}} + \varepsilon^5 \ell_y^{\star 5} \frac{2}{5!} \frac{\partial^5 \Theta_y}{\partial y^{\star 5}} + O(\varepsilon^7), \end{aligned} \tag{21}$$

$$\begin{aligned} &-u_{x(n_x,m_y-1)} + u_{x(n_x,m_y+1)} \\ &\qquad = 2\varepsilon \ell_y^\star \frac{\partial U_x}{\partial y^\star} + \varepsilon^3 \ell_y^{\star 3} \frac{2}{3!} \frac{\partial^3 U_x}{\partial y^{\star 3}} + \varepsilon^5 \ell_y^{\star 5} \frac{2}{5!} \frac{\partial^5 u_x}{\partial y^{\star 5}} + O(\varepsilon^7), \end{aligned} \tag{22}$$

and finally,

$$\begin{aligned} &\theta_{y(n_x,m_y-1)} + 4\theta_{y(n_x,m_y)} + \theta_{y(n_x,m_y+1)} \\ &\qquad = 6\Theta_y + \varepsilon^2 \ell_y^{\star 2} \frac{\partial^2 \Theta_y}{\partial y^{\star 2}} + \varepsilon^4 \ell_y^{\star 4} \frac{2}{4!} \frac{\partial^4 \Theta_y}{\partial y^{\star 4}} + \varepsilon^6 \ell_y^{\star 6} \frac{2}{6!} \frac{\partial^6 \Theta_y}{\partial y^{\star 6}} + O(\varepsilon^8). \end{aligned} \tag{23}$$

By construction, the coefficients of the power expansions for ε in (20)–(23) are of the same dominant order, but also they contain terms of lower order. Therefore, to really order the relative weight of the different addends, it is necessary to introduce the asymptotic expansions of the variables U_x, U_y, Θ_x and Θ_y. This is essential to effectively separate the power exponents and to ensure the coherence of the passage to the limit $\varepsilon \to 0$. It should be noted that consecutive terms of Taylor

expansions are *systematically* offset from ε^2. It is therefore sufficient to introduce the developments in the even powers of ε. Consequently, we are looking for fields U_x, U_y, Θ_x, Θ_y in the generic form

$$U_x = U_x^{(0)} + \varepsilon^2 U_x^{(2)} + \varepsilon^4 U_x^{(4)} + O(\varepsilon^6 U_x^{(6)}).$$

Thereafter, we will denote with a tilde the correction terms that are physically observable, e.g.,

$$\widetilde{U}_x^{(4)} = \varepsilon^4 U_x^{(4)}, \quad \widetilde{\Theta}_x^{(4)} = \varepsilon^4 \Theta_x^{(4)}.$$

Referring the developments in power of ε^2 in (20)–(23), we get

$$\begin{aligned} &u_{x(n_x,m_y-1)} - 2u_{x(n_x,m_y)} + u_{x(n_x,m_y+1)} \\ &\qquad = \varepsilon^2 \ell_y^{\star 2} \frac{\partial^2 U_x^{(0)}}{\partial y^{\star 2}} + \varepsilon^4 \ell_y^{\star 4} \left(\frac{\partial^2 U_x^{(2)}}{\partial y^{\star 2}} + \frac{2}{4!} \frac{\partial^4 U_x^{(0)}}{\partial y^{\star 4}} \right) + O(\varepsilon^6), \end{aligned} \tag{24}$$

$$\begin{aligned} &u_{x(n_x-1,m_y)} - 2u_{x(n_x,m_y)} + u_{x(n_x+1,m_y)} \\ &\qquad = \varepsilon^2 \ell_x^{\star 2} \frac{\partial^2 U_x^{(0)}}{\partial x^{\star 2}} + \varepsilon^4 \ell_x^{\star 4} \left(\frac{\partial^2 U_x^{(2)}}{\partial x^{\star 2}} + \frac{2}{4!} \frac{\partial^4 U_y^{(0)}}{\partial x^{\star 4}} \right) + O(\varepsilon^6), \end{aligned} \tag{25}$$

$$\begin{aligned} &-\theta_{y(n_x,m_y-1)} + \theta_{y(n_x,m_y+1)} \\ &\qquad = \varepsilon \ell_y^{\star} 2 \frac{\partial \Theta_y^{(0)}}{\partial y^{\star}} + \varepsilon^3 \ell_y^{\star 3} \left(2 \frac{\partial \Theta_y^{(2)}}{\partial y^{\star}} + \frac{2}{3!} \frac{\partial^3 \Theta_y^{(0)}}{\partial y^{\star 3}} \right) \\ &\qquad\quad + \varepsilon^5 \ell_y^{\star 5} \left(2 \frac{\partial \Theta_y^{(4)}}{\partial y^{\star}} + \frac{2}{3!} \frac{\partial^3 \Theta_y^{(0)}}{\partial y^{\star 3}} + \frac{2}{5!} \frac{\partial^5 \Theta_y^{(0)}}{\partial y^{\star 5}} \right) + O(\varepsilon^7), \end{aligned} \tag{26}$$

$$\begin{aligned} &-u_{x(n_x,m_y-1)} + u_{x(n_x,m_y+1)} \\ &\qquad = \varepsilon \ell_y^{\star} 2 \frac{\partial U_x^{(0)}}{\partial y^{\star}} + \varepsilon^3 \ell_y^{\star 3} \left(2 \frac{\partial U_x^{(2)}}{\partial y^{\star}} + \frac{2}{3!} \frac{\partial^3 U_x^{(0)}}{\partial y^{\star 3}} \right) \\ &\qquad\quad + \varepsilon^5 \ell_y^{\star 5} \left(2 \frac{\partial U_x^{(4)}}{\partial y^{\star}} + \frac{2}{3!} \frac{\partial^3 U_x^{(2)}}{\partial y^{\star 3}} + \frac{2}{5!} \frac{\partial^5 U_x^{(0)}}{\partial y^{\star 5}} \right) + O(\varepsilon^7), \end{aligned} \tag{27}$$

$$\begin{aligned} &\theta_{y(n_x,m_y-1)} + 4\theta_{y(n_x,m_y)} + \theta_{y(n_x,m_y-1)} \\ &\qquad = 6\Theta_y^{(0)} + \varepsilon^2 \ell_y^{\star 2} \left(\Theta_y^{(2)} + \frac{\partial^2 \Theta_y^{(0)}}{\partial y^{\star 2}} \right) \\ &\qquad\quad + \varepsilon^4 \ell_y^{\star 4} \left(\Theta_y^{(4)} + \frac{\partial^2 \Theta_y^{(2)}}{\partial y^{\star 2}} + \frac{2}{4!} \frac{\partial^4 \Theta_y^{(0)}}{\partial y^{\star 4}} \right) + O(\varepsilon^6). \end{aligned} \tag{28}$$

The calculations presented in this subsection provides an accurate transformation of the finite differences into successive derivatives. This step is essential to get the continuous asymptotic model valid in the limit $\varepsilon \to 0$.

5. Asymptotic macroscopic model

In (24)–(28), the macroscopic continuous fields and their macroscopic derivatives appear. By substituting them in the equilibrium equations (13)–(14) we may obtain a macroscopic continuous formulation of the equilibrium of pivots (equilibrium of force along x and equilibrium of moment for the elements along y). To make explicit which are the appearing powers of ε, it is convenient to write the obtained equations in the nondimensional variables $x^\star$ and $y^\star$, where L is the reference length. As, by hypothesis, ℓ_x and ℓ_y are of order ε with respect to L, we have $\ell_x = \ell_x^\star \ell = \varepsilon \ell_x^\star L$ and $\ell_y = \varepsilon \ell_y^\star L$. Thus, by limiting ourselves to the infinitesimals $O(\varepsilon^6)$, the continuity of moments of the elements oriented along y (14) gives, after grouping different terms,

$$6\left(\frac{\partial U_x^{(0)}}{\partial y^\star} + L\ell_y^\star \Theta_y^{(0)}\right) + \varepsilon^2 \ell_y^{\star 2} 6\left(\frac{\partial U_x^{(2)}}{\partial y^\star} + L\ell_y^\star \Theta_y^{(2)}\right)$$
$$+\varepsilon^4 \ell_y^{\star 4}\left(6\left(\frac{\partial U_x^{(4)}}{\partial y^\star} + L\ell_y^\star \Theta_y^{(4)}\right) + \frac{2}{4!}\frac{\partial^4}{\partial y^{\star 4}}\left(\frac{1}{5}\frac{\partial U_x^{(0)}}{\partial y^\star} + L\ell_y^\star \Theta_y^{(0)}\right)\right) + O(\varepsilon^6) = 0, \quad (29)$$

and the equilibrium of forces along x (13) gives

$$R_x \varepsilon^2 \ell_y^{\star 2}\left(\frac{\partial}{\partial y^\star}\left(\frac{\partial U_x^{(0)}}{\partial y^\star} + L\ell_y^\star \Theta_y^{(0)}\right)\right.$$
$$+\varepsilon^2 \ell_y^{\star 2}\left\{\frac{\partial}{\partial y^\star}\left(\frac{\partial U_x^{(2)}}{\partial y^\star} + L\ell_y^\star \Theta_y^{(2)}\right) + \frac{\partial^3}{\partial y^{\star 3}}\left(\frac{2}{4!}\frac{\partial U_x^{(0)}}{\partial y^\star} + \frac{1}{3!}L\ell_y^\star \Theta_y^{(0)}\right)\right\} + O(\varepsilon^4)\Bigg)$$
$$+\varepsilon^2 \ell_x^{\star 2}\left(\frac{\partial^2 U_x^{(0)}}{\partial x^{\star 2}} + \varepsilon^2 \ell_x^{\star 2}\left\{\frac{\partial^2 U_x^{(2)}}{\partial x^{\star 2}} + \frac{2}{4!}\frac{\partial^4 U_x^{(0)}}{\partial x^{\star 4}}\right\}\right.$$
$$\left.\left.+\varepsilon^4 \ell_x^{\star 4}\left\{\frac{\partial^2 U_x^{(4)}}{\partial x^{\star 2}} + \frac{2}{4!}\frac{\partial^4 U_x^{(2)}}{\partial x^{\star 4}} + \frac{2}{6!}\frac{\partial^6 U_x^{(0)}}{\partial x^{\star 6}}\right\} + O(\varepsilon^6)\right)\right) = 0, \quad (30)$$

where

$$R_x = \frac{12 E_y I_y}{\ell_y^3}\frac{\ell_x}{E_x A_x}.$$

The moment in (29) comes in the form of a series in which the mechanical characteristics of beams do not interfere. The convergence of the series when $\varepsilon \to 0$

implies that each involved term vanishes. Consequently,

$$\frac{\partial U_x^{(0)}}{\partial y^\star} + L\ell_y^\star \Theta_y^{(0)} = 0, \tag{31}$$

$$\frac{\partial U_x^{(2)}}{\partial y^\star} + L\ell_y^\star \Theta_y^{(2)} = 0, \tag{32}$$

$$\frac{\partial U_x^{(4)}}{\partial y^\star} + L\ell_y^\star \Theta_y^{(4)} + \frac{1}{3\cdot 4!}\frac{\partial^4}{\partial y^{\star 4}}\left(\frac{1}{5}\frac{\partial U_x^{(0)}}{\partial y^\star} - L\ell_y^\star \Theta_y^{(0)}\right) = 0. \tag{33}$$

This precisely means that the equilibrium of moments for y fibers requires, with an error being equal to $O(\varepsilon^4)$, a relationship between their rotation and their transverse gradient, which is expressed in the dimensional fields as

$$\frac{\partial U_x}{\partial y} + \ell_y^\star \Theta_y = O(\varepsilon^4).$$

At the dominant order, Θ_y can thus be considered a *hidden* variable which does not emerge in the macroscopic description at the leading order. Only by considering the correction $O(\varepsilon^4)$ does the rotation differ from the transverse gradient because we have

$$\frac{\partial U_x^{(4)}}{\partial y^\star} + L\ell_y^\star \Theta_y^{(4)} = -\frac{2}{5!}\frac{\partial^5 \partial U_x^{(0)}}{\partial y^{\star 5}},$$

or, in dimensional variables and denoting explicitly the observable corrections $\widetilde{U}_x^{(4)} = \varepsilon^4 U_x^{(4)}$, $\widetilde{\Theta}_x^{(4)} = \varepsilon^4 \Theta_x^{(4)}$:

$$\frac{\partial \widetilde{U}_x^{(4)}}{\partial y} + \ell_y \widetilde{\Theta}_y^{(4)} = -\ell^4 \frac{2}{5!}\frac{\partial^5 \partial U_x^{(0)}}{\partial y^5}.$$

Let us now replace (31)–(32) in the balance equation (30). This leads to

$$R_x \varepsilon^2 \ell_y^{\star 4}\left(\frac{2}{4!}\frac{\partial^4 U_x^{(0)}}{\partial y^{\star 4}} + O(\varepsilon^4)\right) = \ell_x^{\star 2}\left(\frac{\partial^2 U_x^{(0)}}{\partial x^{\star 2}} + \varepsilon^2 \ell_x^{\star 2}\left\{\frac{\partial^2 U_x^{(2)}}{\partial x^{\star 2}} + \frac{2}{4!}\frac{\partial^4 U_x^{(0)}}{\partial x^{\star 4}}\right\}\right) + O(\varepsilon^4). \tag{34}$$

To exploit this equation, it is necessary to weigh the effects of bending (left-hand side term) and extension (right-hand side term). These effects are a consequence of both the mechanical properties of considered system and of the nature of the admitted kinematics. The mechanical parameters which we choose will introduce the high contrast condition (8), which is expressed by

$$R_x = R_x^\star \varepsilon^2. \tag{35}$$

Regarding the nature of the macroscopic kinematics, we are led thus to distinguish between low or high contrast situations in the axial and the transverse gradient.

5.1. ***Low contrast between axial and transverse gradient of U_x.*** We consider here macroscopic kinematics where axial and transverse components of the displacement gradient U_x are of the same order, i.e.,

$$\frac{\partial U_x^{(0)}}{\partial x^\star} = O\left(\frac{\partial U_x^{(0)}}{\partial y^\star}\right). \tag{36}$$

This estimate explicitly means that the axial and transverse variations have as a common evolution characteristic value $O(L)$. This hypothesis is usually considered in the case of an elastic composite medium where the terms of the strain tensor components are assumed to be of the same order. In this case, we obtain successively (each relative to the orders ε^0, ε^2, ε^4)

$$\begin{aligned}
\frac{\partial^2 U_x^{(0)}}{\partial x^{\star 2}} &= 0,\\
\frac{\partial^2 U_x^{(2)}}{\partial x^{\star 2}} + \frac{2}{4!}\frac{\partial^4 U_x^{(0)}}{\partial x^{\star 4}} &= 0,\\
\frac{\partial^2 U_x^{(4)}}{\partial x^{\star 2}} + \frac{2}{4!}\frac{\partial^4 U_x^{(2)}}{\partial x^{\star 4}} + \frac{2}{6!}\frac{\partial^6 U_x^{(0)}}{\partial x^{\star 6}} &= (\ell_x^\star)^{-2} R_x^\star \ell_y^{\star 4}\frac{2}{4!}\frac{\partial^4 U_x^{(0)}}{\partial y^{\star 4}}.
\end{aligned}$$

By simplifying and returning to the dimensional variables and observable correctors, we deduce that

$$\frac{E_x A_x}{\ell_y}\frac{\partial^2 U_x^{(0)}}{\partial x^2} = 0, \tag{37}$$

$$\frac{E_x A_x}{\ell_y}\frac{\partial^2 \widetilde{U}_x^{(2)}}{\partial x^2} = 0, \tag{38}$$

$$\frac{E_x A_x}{\ell_y}\frac{\partial^2 \widetilde{U}_x^{(4)}}{\partial x^2} = \frac{E_y I_y}{\ell_x}\frac{\partial^4 U_x^{(0)}}{\partial y^4}. \tag{39}$$

Equations (37)–(38) mean that the tension of the fibers oriented along x is *constant* to the accuracy ε^4. Only by considering the order 4 of the correctors, the tension of the beams varies due to the bending of orthogonal beams, as indicated by (39).

The assumption (36) obviously can not cover all cases of loading. In particular, it is not predictive if the lattice is subjected to a uniaxial extension in a direction that does not coincide with one of the directions of the fibers' arrays (see Figure 2). Indeed, if one considers the "red" fiber in Figure 2 (which presents experimental evidence), it is clear that its state of tension cannot be constant; its tension is not vanishing in the clamping but it clearly vanishes at the free end. To describe these

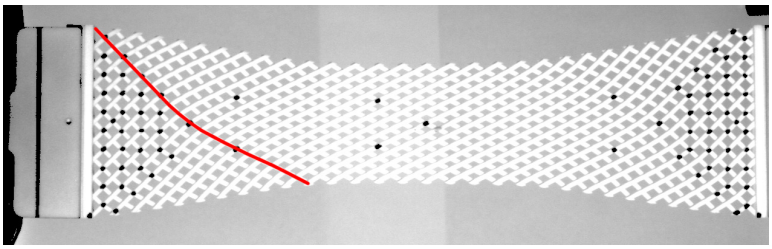

Figure 2. An example of standard bias extension test, courtesy of Tomasz Lekszycki, Marek Pawlikowski and Roman Grygoruk.

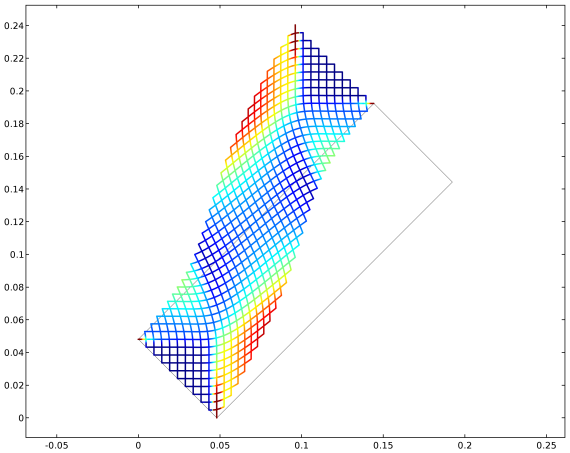

Figure 3. An example of generalized bias test while imposing a shear displacement.

situations it is necessary to change the too restrictive hypothesis (36) by allowing a strong contrast between the axial and transverse components of the gradient of the macroscopic displacement.

5.2. ***Strong contrast between axial and transverse gradient of U_x.*** Thus we are lead to consider macroscopic kinematics where the transverse gradient $\partial U_x^{(0)}/\partial y^\star$ dominates in comparison to the axial gradient $\partial U_x^{(0)}/\partial x^\star$, i.e.,

$$\frac{\partial U_x^{(0)}}{\partial x^\star} \ll \frac{\partial U_x^{(0)}}{\partial y^\star}. \tag{40}$$

This assumption reflects the fact that the axial characteristic length of variation of U_x (denoted $L_{x,a}$) is much larger than the transverse (denoted $L_{x,t}$) length (see, e.g., experimental evidence presented in [dell'Isola et al. 2016d]). This is a consequence of the high shear deformability of the pantographic network compared to its deformability in the axis of the fibers.

To assure scale separation, we are thus lead to consider as a reference length the smaller between the two, i.e., $L = L_{x,t}$, so that

$$\frac{\partial^i U_x^{(0)}}{\partial x^{\star i}} = \frac{O(U_x^{(0)})}{(L_{x,a}/L)^i} = O(U_x^{(0)})\left(\frac{L_{x,t}}{L_{x,a}}\right)^i, \quad \frac{\partial^j U_x^{(0)}}{\partial y^{\star j}} = \frac{O(U_x^{(0)})}{(L_{x,t}/L)^j} = O(U_x^{(0)}).$$

Once we consider $L_{x,t} = \varepsilon^2 L_{x,a}$, we have

$$\frac{\partial U_x^{(0)}}{\partial x^\star} = \varepsilon^2 O\left(\frac{\partial U_x^{(0)}}{\partial y^\star}\right), \tag{41}$$

$$\frac{\partial^2 U_x^{(0)}}{\partial x^{\star 2}} = \varepsilon^4 O\left(\frac{\partial^4 U_x^{(0)}}{\partial y^{\star 4}}\right). \tag{42}$$

The presence of a contrast in the components of the strain tensor as given by (41) is unconventional in elastic composite mediums but arises naturally in the case of weakly compressible viscous fluid (where the trace of the strain rate tensor is negligible compared to its deviatoric component) or in beams and plates (where deformations in the section of the beam — or in the thickness of the plate — are negligible). This contrast is present also in pantographic sheets.

Replacing the estimate (42) into (34) we get at the leading order

$$\frac{\partial^2 U_x^{(0)}}{\partial x^{\star 2}} = (\ell_x^\star)^{-2} R_x^\star \ell_y^{\star 4} \frac{2}{4!} \frac{\partial^4 U_x^{(0)}}{\partial y^{\star 4}},$$

or, returning to the dimensional variables and normalizing by introducing the surface of the periodic cell, we have

$$\frac{E_x A_x}{\ell_y} \frac{\partial^2 U_x^{(0)}}{\partial x^2} = \frac{E_y I_y}{\ell_x} \frac{\partial^4 U_x^{(0)}}{\partial y^4}. \tag{43}$$

This equation indicates that the normal force (left-hand side) varies *at the first order* in the beams due to the shear force exerted by the orthogonal beams (right-hand side). This is made possible because the transverse gradient is of *two orders of magnitude higher* than that of the extension gradient (see again (41)).

Moreover, we note that (43) is more general than (37) and it is needed in the considered mechanical system. Moreover, (43) degenerates to the (37) when $\partial U_x^{(0)}/\partial x \gg \varepsilon^2 \partial U_x^{(0)}/\partial y$. We will use in what follows the description (43), which applies to more general kinematics.

5.3. ***Synthesis of obtained results.*** The above results, derived from the system (13)–(14) for the variables $U_x^{(0)}$ and $\Theta_y^{(0)}$ is transposed by a similar analysis of the system (15)–(16) to the variables $U_y^{(0)}$ and $\Theta_x^{(0)}$. The description in small deformations of the orthogonal pantographic lattice is therefore obtained by restricting the analysis to *the dominant order* (for simplicity, the exponents of order $^{(0)}$ are

removed):

$$\frac{E_x A_x}{\ell_y}\frac{\partial^2 U_x}{\partial x^2} = \frac{E_y I_y}{\ell_x}\frac{\partial^4 U_x}{\partial y^4}, \tag{44}$$

$$\frac{E_y A_y}{\ell_x}\frac{\partial^2 U_y}{\partial y^2} = \frac{E_x I_x}{\ell_y}\frac{\partial^4 U_y}{\partial x^4}, \tag{45}$$

with the addition of the relationships between the transverse gradients and rotations:

$$\frac{\partial U_x}{\partial y} + \sqrt{\frac{\ell_y}{\ell_x}}\Theta_y = 0, \quad \frac{\partial U_y}{\partial x} - \sqrt{\frac{\ell_x}{\ell_y}}\Theta_x = 0. \tag{46}$$

Remark that (44)–(45) can be rewritten by introducing two intrinsic characteristic lengths η_x and η_y as follows:

$$\frac{\partial^2 U_x}{\partial x^2} = \eta_x^2 \frac{\partial^4 U_x}{\partial y^4}, \quad \frac{\partial^2 U_y}{\partial y^2} = \eta_y^2 \frac{\partial^4 U_y}{\partial x^4},$$

where

$$\eta_x^2 := \frac{\ell_y E_y I_y}{\ell_x E_x A_x}, \quad \eta_y^2 := \frac{\ell_x E_x I_x}{\ell_y E_y A_y}.$$

It is clear that the physics of the system is governed by these internal intrinsic lengths which differ from the size of the cell.

The model governed by (44)–(45) is of the type of a conservative generalized continuum medium having deformation energy that depends on first- and second-order gradients of displacement (see [Alibert et al. 2003; Seppecher et al. 2011]). Its evolution is ruled by two displacement fields which are *independent and uncoupled*, i.e., U_x and U_y. This particular behavior is within the framework of the second gradient continua where the internal actions are described by a stress symmetric tensor $\boldsymbol{T}$ of order two and by a hyperstress tensor $\mathcal{T}$ of third order. To make the identification, we pose (44)–(45) in the following form, where the differential operator DIV denotes the Lagrangian divergency:

$$\mathrm{DIV}(\boldsymbol{T} - \mathrm{DIV}(\mathcal{T})) = 0, \tag{47}$$

and where we used the definitions

$$\boldsymbol{T} := \tfrac{1}{2} C \,.\, (\nabla \boldsymbol{U} + \nabla \boldsymbol{U}^{\mathrm{t}}), \quad \mathcal{T} := D \,.\, \nabla\nabla \boldsymbol{U} \tag{48}$$

in which the symbol "." denotes the repeated index saturation between different order tensors and superscript "t" the transposition of second-order tensors. The elasticity tensors C and D of order four and six respectively have the particular

form defined by their components as

$$C_{abcd} := \frac{E_x A_x}{\ell_y}\delta_{ax}\delta_{bx}\delta_{cx}\delta_{dx} + \frac{E_y A_y}{\ell_x}\delta_{ay}\delta_{by}\delta_{cy}\delta_{dy}, \tag{49}$$

$$D_{abcdef} := \frac{E_y I_y}{\ell_x}\delta_{ax}\delta_{by}\delta_{cy}\delta_{dx}\delta_{ey}\delta_{fy} + \frac{E_x I_x}{\ell_y}\delta_{ay}\delta_{bx}\delta_{cx}\delta_{dy}\delta_{ex}\delta_{fx}. \tag{50}$$

Remark that (separately) the tensors C and D are not coercive. For instance, pure shear deformations do not have any first gradient energetic content, while any affine displacement field does not have any second gradient energetic content. This is consistent with the existence, for pantographic sheets, of floppy modes as nullifiers of deformations energy, in addition to the standard rigid motions. Nevertheless, considering both first and second gradient energies together, the system can be qualified as "subcoercive" when suitable boundary conditions are imposed in such a way that floppy modes are excluded. In the framework of this requirement, the set of admissible displacements is restricted if compared to the one needed in first gradient theory, where only rigid body motions are excluded. We conjecture that in the set of considered admissible displacements, the total deformation energy is definite positive and leads to well-posed problems. This seems physically well-grounded and is confirmed by all the performed numerical simulations presented in the last section.

To identify the class of physically meaningful boundary conditions, in the next section we more closely study the structure of the considered energy.

5.4. ***Energy formulation and boundary conditions for pantographic lattices.*** The general framework of second gradient continua (as formulated in [dell'Isola et al. 2015c]) enables, by means of the energy formulation and of the divergence theorem, to specify the boundary conditions which can be consistently considered as applicable to them.

Let $\mathcal{B}$ be a bidimensional medium whose elastic energy depends upon the displacement gradient $\nabla \boldsymbol{U}$ acting on the second-order stress tensor $\boldsymbol{T}$ and upon the second displacement gradient acting on the third-order hyperstress tensor $\mathcal{T}$. In this case the energy W of $\mathcal{B}$ is

$$2W = \int_{\mathcal{B}} (\boldsymbol{T} : \nabla \boldsymbol{U} + \mathcal{T} \vdots \nabla\nabla \boldsymbol{U}) \tag{51}$$

Transforming this expression through successive integrations by parts enables us to make the link between the variation of internal energy and the energy supplied at the boundary of $\mathcal{B}$ (see, e.g., [dell'Isola et al. 2015c]). As the considered system is bidimensional, the boundary consists of a set of regular edges ∂B with unit normal $\boldsymbol{n}$ and wedges $\partial\partial\mathcal{B}$ consisting of the union of a finite number N of vertices S_I, i.e.,

$\partial\partial\mathcal{B} = \cup S_I = \{S\}$. For our calculations we introduce Levi-Civita tensorial notation, keeping track of the covariance and contravariance nature of the considered tensorial quantities and we use Latin indices for Eulerian components and Greek letters for Lagrangian components. Therefore, we have

$$\begin{aligned}
\delta W &= \int_{\mathcal{B}} (\boldsymbol{T} : \nabla\delta\boldsymbol{U} + \mathcal{T} \vdots \nabla\nabla\delta\boldsymbol{U}) = \int_{\mathcal{B}} (T_i^{\beta}\delta U^i_{,\beta} + \mathcal{T}_i^{\alpha\beta}\delta U^i_{,\alpha\beta}) \\
&= \int_{\mathcal{B}} (-T^{\alpha}_{i,\alpha}\delta U^i - \mathcal{T}^{\alpha\beta}_{i,\beta}\delta U^i_{,\alpha}) + \int_{\mathcal{B}} (T_i^{\beta}\delta U^i + \mathcal{T}_i^{\alpha\beta}\delta U^i_{,\alpha})_{,\beta} \\
&= \int_{\mathcal{B}} (-T^{\alpha}_{i,\alpha}\delta U^i - \mathcal{T}^{\alpha\beta}_{i,\beta}\delta U^i_{,\alpha}) + \int_{\partial\mathcal{B}} (T_i^{\beta}\delta U^i + \mathcal{T}_i^{\alpha\beta}\delta U^i_{,\alpha})n_{\beta} \\
&= \int_{\mathcal{B}} (\mathcal{T}^{\alpha\beta}_{i,\beta\alpha} - T^{\alpha}_{i,\alpha})\delta U^i + \int_{\partial\mathcal{B}} \big((T_i^{\beta} - \mathcal{T}^{\beta\alpha}_{i,\alpha})\delta U^i + \mathcal{T}_i^{\alpha\beta}\delta U^i_{,\alpha}\big)n_{\beta}.
\end{aligned} \tag{52}$$

Using the equilibrium equation (47), the first integral in the right-hand side vanishes. Furthermore, the last term of the second integral can be decomposed into a tangent and a normal contribution. As the considered system is bidimensional, the boundary ∂B includes a set of regular edges. Thus, introducing the projector on the tangent direction of ∂B, $P = I - n\otimes n$ (hence $P^{\gamma}_{\alpha} = \delta^{\gamma}_{\alpha} - n_{\alpha}n^{\gamma}$ and $P \,.\, P = P$), we have

$$\begin{aligned}
\delta W &= \int_{\partial\mathcal{B}} \big((T_i^{\beta} - \mathcal{T}^{\beta\alpha}_{i,\alpha})n_{\beta}\delta U^i + (\mathcal{T}_i^{\alpha\beta}n_{\alpha}n_{\beta})\delta U^i_{,\gamma}n^{\gamma} + \mathcal{T}_i^{\alpha\beta}n_{\beta}P^{\delta}_{\alpha}\delta U^i_{,\gamma}P^{\gamma}_{\delta}\big) \\
&= \int_{\partial\mathcal{B}} \big((T_i^{\beta} - \mathcal{T}^{\beta\alpha}_{i,\alpha})n_{\beta}\delta U^i + (\mathcal{T}_i^{\alpha\beta}n_{\alpha}n_{\beta})\delta U^i_{,\gamma}n^{\gamma} \\
&\qquad + (\mathcal{T}_i^{\alpha\beta}n_b P^{\delta}_{\alpha}\delta U^i)_{,\gamma}P^{\gamma}_{\delta} - (\mathcal{T}_i^{\alpha\beta}n_{\beta}P^{\delta}_{\alpha})_{,\gamma}P^{\gamma}_{\delta}\delta U^i\big) \\
&= \int_{\partial\mathcal{B}} \big((T_i^{\beta} - \mathcal{T}^{\beta\alpha}_{i,\alpha})n_{\beta} - (\mathcal{T}_i^{\alpha\beta}n_{\beta}P^{\delta}_{\alpha})_{,\gamma}P^{\gamma}_{\delta}\big)\delta U^i + \int_{\partial\mathcal{B}} (\mathcal{T}_i^{\alpha\beta}n_{\alpha}n_{\beta})\delta U^i_{,\gamma}n^{\gamma} \\
&\qquad + \int_{\partial\partial\mathcal{B}} \mathcal{T}_i^{\alpha\beta}n_{\beta}P^{d}_{\alpha}N_{\delta}\delta U^i.
\end{aligned} \tag{53}$$

On the last integral on $\partial\partial B = \{S\}$, the vectors $\boldsymbol{n}$ and $\boldsymbol{N}$ take the values $\boldsymbol{n}^{\pm}$ and $\boldsymbol{N}^{\pm}$ defined on the both sides of the discontinuity of the edges. This is also the case for $\mathcal{T}$ and P. On each side, the vector $\boldsymbol{N}$ is the tangent vector to ∂B which is the outer pointing normal to the border of ∂B; see Figure 4. Thus $P^{+} \,.\, \boldsymbol{N}^{+} = \boldsymbol{N}^{+}$ and $P^{-} \,.\, \boldsymbol{N}^{-} = \boldsymbol{N}^{-}$. In a condensed way, we can write (where the symbol $_{||}$ refers to the tangent projection of a tensor on ∂B)

$$\begin{aligned}
&\int_{\mathcal{B}} (\boldsymbol{T} : \nabla\delta\boldsymbol{U} + \mathcal{T} \vdots \nabla\nabla\delta\boldsymbol{U}) \\
&= \int_{\partial\mathcal{B}} ((T - \mathrm{DIV}\,\mathcal{T}) \,.\, n - \mathrm{DIV}_{||}\,\mathcal{T}_{||}) \,.\, \delta U + (\mathcal{T} \,.\, n \,.\, n)\delta\frac{\mathrm{d}U}{\mathrm{d}n} + \sum_{\{S\}} [\mathcal{T} \,.\, n \,.\, N] \,.\, \delta U
\end{aligned} \tag{54}$$

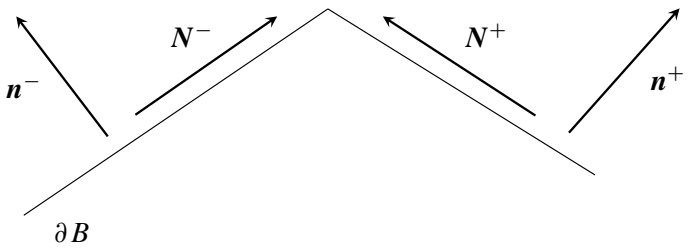

Figure 4. Sketch of vectors $\boldsymbol{n}$ and $\boldsymbol{N}$ on the boundaries.

with

$$[\mathcal{T} \,.\, n \,.\, N] = (\mathcal{T}^+ \,.\, n^+ \,.\, N^+) + (\mathcal{T}^- \,.\, n^- \,.\, N^-).$$

The previous integration by parts implies that in order to have well-posed problems, one has to suitably assign boundary conditions in a specific way (see, e.g., [Mindlin 1964]). In particular, on any regular point belonging to the set of edges $\partial\mathcal{B}$ one can assign:

- either a component U^i or its dual quantity $(T_i^b - \mathcal{T}_{i,\alpha}^{\beta\alpha})n_\beta - (\mathcal{T}_i^{\alpha\beta} n_\beta P_\alpha^\delta)_{,\gamma} P_\delta^\gamma$. In the case of the rectilinear edge $\partial\mathcal{B}$ the normal and the projector are constants and this expression simplifies into $(T_i^\beta - \mathcal{T}_{i,\alpha}^{\beta\alpha} - \mathcal{T}_{i,\gamma}^{\alpha\beta}(\delta_\alpha^\gamma - n_\gamma n_\alpha))n_\beta$;
- either a component of displacement normal gradient, $\mathrm{d}U^i/\mathrm{d}n$, or its dual quantity $(\mathcal{T}_i^{\alpha\beta} n_a n_\beta)$.

Moreover, on vertices constituting $\partial\partial B = \{S\}$ one can assign:

- either a component U^i or its dual quantity $[\mathcal{T}_i^{\alpha\beta} n_b N_\alpha]$ which expresses the discontinuity of the wedge on the vertices (see Figure 4).

Therefore the weak condition for equilibrium is given by

$$\delta W = \int_{\partial\mathcal{B}} f_i^{\mathrm{ext}} \delta U^i + \tau_i^{\mathrm{ext}} \delta U^i_{,\gamma} n^\gamma + \int_{\partial\partial\mathcal{B}} F_i^{\mathrm{ext}} \delta U^i, \tag{55}$$

where external actions are given by forces per unit line f_i^{ext} but also by concentrated forces on vertices F_i^{ext} and by double forces per unit line τ_i^{ext} (see [Germain 1973]).

One can apply these results to the particular pantographic lattice considered, where the preferred orthogonal directions x and y coincide with the array of material fibers. In the context of small deformations, the Lagrangian and Eulerian coordinate systems can be identified. In the pantographic case given by (49) and (50) the deformation energy is given by

$$2W = \int_{\mathcal{B}} \left(\frac{E_x A_x}{\ell_y}(U^x_{,x})^2 + \frac{E_y A_y}{\ell_x}(U^y_{,y})^2 + \frac{E_y I_y}{\ell_x}(U^x_{,yy})^2 + \frac{E_x I_x}{\ell_y}(U^y_{,xx})^2 \right) \mathrm{d}x\,\mathrm{d}y \tag{56}$$

so we have that, as $\boldsymbol{T} = \partial W/\partial \nabla U$ and $\mathcal{T} = \partial W/\partial \nabla\nabla U$, the only nonvanishing components of stress and hyperstress are

$$T_x^x = \frac{E_x A_x}{\ell_y} U^x_{,x}, \qquad T_y^y = \frac{E_y A_y}{\ell_x} U^y_{,y},$$
$$\mathcal{T}_y^{xx} = \frac{E_x I_x}{\ell_y} U^y_{,xx}, \quad \mathcal{T}_x^{yy} = \frac{E_y I_y}{\ell_x} U^x_{,yy}.$$

Thus, for the pantographic sheet, the two types of kinematic and static (more often called natural) boundary conditions which apply to a straight line edge of normal $\boldsymbol{n} = n_x \boldsymbol{e}_x + n_y \boldsymbol{e}_y$ take the following form:

$$U^x \text{ dual of } T_x^x n_x + (-\mathcal{T}^{yy}_{x,y}(1+n_x^2) + \mathcal{T}^{yy}_{x,x} n_x n_y) n_y, \quad \frac{\mathrm{d}U^x}{\mathrm{d}n} \text{ dual of } \mathcal{T}_x^{yy} n_y^2,$$
$$U^y \text{ dual of } T_y^y n_y + (-\mathcal{T}^{xx}_{y,x}(1+n_y^2) + \mathcal{T}^{xx}_{y,y} n_x n_y) n_x, \quad \frac{\mathrm{d}U^y}{\mathrm{d}n} \text{ dual of } \mathcal{T}_y^{xx} n_x^2.$$

On the vertices, noting that $\boldsymbol{n}$ and $\boldsymbol{N}$ are orthogonal, the flux dual to the displacement components U^x and U^y are respectively $\mathcal{T}_x^{-yy} n_x^- n_y^- - \mathcal{T}_x^{+yy} n_x^+ n_y^+$ and $\mathcal{T}_y^{-xx} n_x^- n_y^- - \mathcal{T}_y^{+xx} n_x^+ n_y^+$. Remark that they vanish when the vertex angle is $\frac{1}{2}\pi$ and the boundary is parallel to the fibers.

For a better physical insight, consider for instance a straight edge oriented along the direction x, then $\boldsymbol{n} = \boldsymbol{e}_y$ and the boundary condition simplifies to

$$U^x \text{ dual of } -\mathcal{T}^{yy}_{x,y} = -\frac{E_y I_y}{\ell_x} U^x_{,yyy}, \quad \frac{\mathrm{d}U^x}{\mathrm{d}y} \text{ dual of } \mathcal{T}_x^{yy} = \frac{E_y I_y}{\ell_x} U^x_{,yy},$$
$$U^y \text{ dual of } T_y^y = \frac{E_y A_y}{\ell_x} U^y_{,y}, \qquad \frac{\mathrm{d}U^y}{\mathrm{d}y} \text{ dual of } \mathcal{T}_y^{xx} n_x^2 = 0.$$

These boundary conditions on the lattice can be easily understood by recalling standard beam theory. They show this:

- A virtual displacement tangent to the fiber materializing the edge develops energy due to the shear forces in the orthogonal fibers.
- A virtual displacement normal to the edge fiber develops energy due to the tension forces in the orthogonal fibers.
- A rotation of the edge fiber develops energy due to the couple in the orthogonal fibers.
- No energy is developed (in small deformations) by the extension of the orthogonal fibers associated with the couple of the edge fiber.

If the vertex at the end of the edge along x presents an internal angle α, the static quantities dual to the components U^x and U^y are respectively the weighted couples $\mathcal{T}_x^{+yy} \frac{1}{2} \sin(2\alpha)$ and $-\mathcal{T}_y^{+xx} \frac{1}{2} \sin(2\alpha)$. No energy is developed if the vertex angle is $\frac{1}{2}\pi$ with edges oriented along the fibers.

A similar interpretation applies when the straight edge presents an angle with the fiber orientation; however, due to the coupling between the forces and couples in different directions, the physical interpretation of the boundary condition becomes more difficult.

In this paper, for the sake of simplicity, we consider only imposed boundary conditions on displacements and displacement gradients and we consider weak form (55) of equilibrium conditions, so that no dual boundary conditions (on forces or double forces) are assigned. In further papers, we will consider more general situations.

6. Some equilibrium shapes of linear pantographic sheets: numerical simulations

Pantographic sheets have an exotic behavior which is not only characterized by their anisotropy as evidenced by:

(1) their vanishing resistance to shear deformation, and

(2) their significant resistance to elongation along fibers, and also by their capacity to resist variations in their so-called "geodesic curvature" (see [dell'Isola and Steigmann 2015; Steigmann and dell'Isola 2015; Giorgio et al. 2015; Giorgio et al. 2016]), i.e., the changes of curvature of material curves induced by in-plane displacements.

Moreover, in their deformation patterns one can observe the onset of inner boundary layers where bending of constituting beams is concentrated, as suggested by the existence of the intrinsic characteristic lengths η_x and η_y.

The aim of this section is to provide numerical illustrations of the theoretical developments presented in the previous sections. The considered examples may seem purely academic or dictated simply by the taste of investigating mathematical structures (see [Dieudonné 1987]). Although we indeed consider that scientific knowledge is based on the study of exemplary cases; see [Russo 2004; Hero/Woodcroft 1851; Heath 1921a; 1921b; Archimedes/Heath 1897; 1912]. In addition, a potential application of the presented results concern the forming of fiber reinforced composites (see, e.g., [Cao et al. 2008; Launay et al. 2008; d'Agostino et al. 2015; Harrison 2016; Abdiwi et al. 2013; Nikopour and Selvadurai 2014]).

All the presented numerical simulations are obtained by a code created using COMSOL Multiphysics. The homogenized energy introduced in this paper (56) is minimized by using the package "Weak Form PDE" and by introducing standard third-order Hermite finite elements. While the used code is surely not optimized for the introduced problem (we believe that the recently developed numerical methods would be more efficient, see, e.g., [Cazzani et al. 2016a; 2016b; Greco and Cuomo 2013; 2014; 2015; 2016; Turco and Aristodemo 1998; Beirão da Veiga

et al. 2008; Della Corte et al. 2016]), its rate of convergence seems satisfactory for getting preliminary results concerning the behavior of the simplest structures; actually, it is based on the introduction of an auxiliary tensor field which appears in the deformation energy and is equated to the displacement gradient by means of suitable fields of Lagrange multipliers. Remark also that all presented numerical simulations are really and intrinsically mesh-independent, because of the properties of the introduced continuum model, where the second gradient of displacement is at the same time modeling the relevant physical properties and supplies a regularizing effect on equilibrium equations.

In the presented simulations we have chosen a lattice made of square cells, so that $\ell_x = \ell_y = \ell$ and we have imposed that the x and y fibers have identical rectangular sections (having sides a and b) and elastic moduli so that $E_y = E_x$, $I_x = I_y = \frac{1}{12}ba^3$ and $A_x = A_y = ab$. As a consequence we have that

$$\eta^2 = \eta_x^2 = \eta_y^2 = \frac{I_x}{A_x} = \frac{I_y}{A_y} = \tfrac{1}{12}a^2.$$

The values $a = 0.9\,\text{mm}$ and $b = 1.6\,\text{mm}$ are used for pantographic structures, following experimental measurements (see [dell'Isola et al. 2015b]) having rectangular sections. Young's modulus is 1600 MPa. We remark that the elastica model for beams is applicable in the considered situation as $\ell = 4.95\,\text{mm}$ and the number of cells is sufficiently large ($L = 42.42 \times \ell$) to apply the homogenized model.

In the following subsections, we present the numerical simulation of bias tests in different configurations. First, we consider rectangular specimens undergoing standard bias test in extension, but also in shear and bending. The results demonstrate the ability of the model to catch the occurrence of highly nonhomogeneous deformation patterns with inner boundary layer, and illustrate the dependance of the pattern on the different imposed deformations. Second, the same type of bias tests are performed on circular specimens in order to investigate the role of the sample geometry on the equilibrium shape and on the elastic energy distribution. Finally, extension and bending bias tests on circular specimens with a central squared of different orientations are simulated. The comparison with the previous cases evidence the effect of different boundary conditions.

In all the following figures, the black lines indicate the local actual orientation of the material fibers (which are orthogonal in the reference configuration), and the deformed shape is displayed together with the map of the stored energy density. All the calculations are performed in the framework of small deformations; however, for a better insight, the deformation is magnified in the figures.

6.1. ***Bias tests on rectangular pantographic sheet.*** We start by considering a pantographic sheet having a rectangular initial shape with the long side three times longer than the short one.

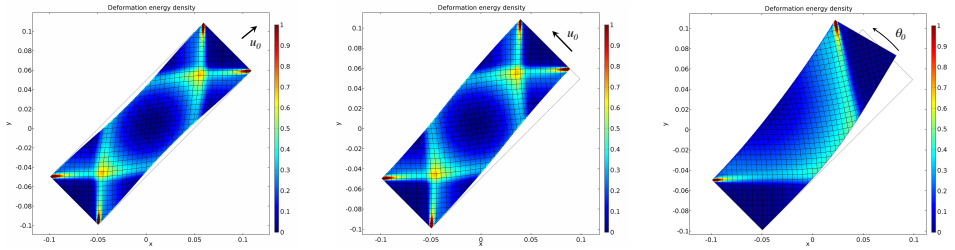

Figure 5. Equilibrium shapes of rectangular specimens submitted to extension (left) shear (center) and bending (right) displacement. The colors indicate the levels of stored energy density.

In the standard extension bias test the short sides are rigidly displaced in the direction of the long side. Figure 5, left, shows the small deformation pattern. Remark that the deformation energy is concentrated along the material lines constituted by some fibers and that, while the fibers are extensible in the present case, the structure of the deformed shape is similar to the one described by Pipkin [1980; 1981] in the case of inextensible fibers. Notice also that the distribution of deformation is strongly nonhomogeneous while respecting the symmetry of the loading. The simulation enables the identification of several zones with different kinematics. The partitioning of the specimen can be described as follows:

– The clamping zones that consists of two "isosceles triangles" with bases on the short sides. These areas do not sustain any significant deformation, neither in extension nor in shear, so the first gradient description (37) applies. The vanishing stored energy results here from the quasirigid body motion of these regions.

– The deformed zones outside of the aforementioned triangles, in which large shear deformations arise. In this highly sheared domain, the behavior is governed by the second gradient description (44)–(45). One distinguishes a central and four lateral subdomains of vanishing stored energy delimited by transition zones. The different subdomains correspond to the occurrence of local "floppy" modes. Indeed, because of the specific boundary condition, "floppy" modes on the whole specimen are forbidden. Nevertheless, the minimum of energy is attained by activating local floppy modes, far from the boundary conditions. This results in large parts of the body where the deformation energy is very close to vanishing.

– The transition zones between the different domains (of quasifloppy modes or quasimonolithic type) consist in the inner boundary layers where the bending of the fibers is concentrated to accommodate the different kinematics that prevails in the two regions in contact. Such layers, which concentrate the

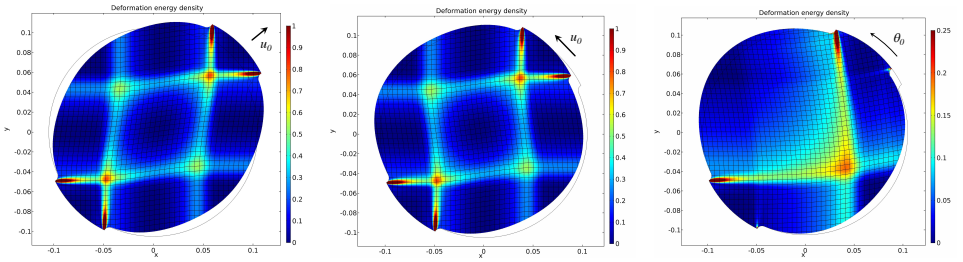

Figure 6. Equilibrium shapes of circular specimens submitted to extension (left) shear (center) and bending (right) displacement. The colors indicate the levels of stored energy density.

elastic energy, take place along material lines constituted by fibers and are characterized by large gradients of shear deformation. These specific features are the direct signature of the second gradient effects: a standard Cauchy continuum description (i.e., simple gradient description, as in (37)) would lead to a homogeneous deformation pattern and avoid the development of shear bands.

Furthermore, the qualitative and quantitative comparison of the numerical simulations plotted on Figure 5, left, and the experimental data presented in [dell'Isola et al. 2015b] clearly argue in favor of the second gradient description (44)-(45) for two reasons. First, the experimental deformation pattern is obviously nonhomogeneous with inner boundary layers whose structure presents a similar geometry as that observed in the simulation. Second, by making a best fit of the experimental data [dell'Isola et al. 2015b], the effective parameters of the second gradient continuum model have been identified. It happens that this "blind" procedure supplies exactly the same values of the effective parameters as the one calculated from the micro-macro upscaling procedure, once the geometric and mechanical properties of the cell beams of the sheet tested experimentally are taken.

In addition, simulations of shear bias tests with uniform lateral displacement imposed on the top side and bending bias tests with rotational displacement imposed on the top side (corresponding to a rigid body rotation centered in the middle of the specimen) have been done. The results are displayed in Figure 5, center and right, respectively. Similar general comments as done for the extension test still apply; however, the geometry of the shear bands and the energy distribution is modified. In particular, the partitioning of the specimen submitted to bending shows only one subdomain of quasifloppy mode which is confined between two quasimonolithic zones.

6.2. ***Bias test on circular pantographic sheets.*** Consider now the same bias test as the previous one, except that the rectangular pantographic sheet is replaced by a

sheet of circular initial shape. The imposed deformations are obtained by clamping one circular arc and imposing a rigid displacement on the opposite one.

In Figure 6, left, we consider the extension imposed by a relative rigid translation of the two arcs in the direction of the common bisecting diameter. Note the great similarity of the deformation pattern obtained with rectangular and circular sheets, when focusing on the internal rectangular domain considered in the standard bias test. This means that, independently of rectangular or circular geometry of the sheet, the structure of the deformation pattern is kept (almost) unchanged when identical kinematic boundary conditions are imposed. Remark also that the largest lateral dimension of the circular sheet enables the inner boundary layers to extend and intersect. Thus the partitioning of the specimen is complemented by the appearance of two additional lateral subdomains.

These observations indicate that in the considered cases, the structure of the inner boundary layer (hence of the partitioning) mostly results from the geometry of the boundary conditions, while the extension of the shear bands depends on the geometry of the whole body. Furthermore, in the circular case, the activation of the deformation outside of the rectangle implies additional energy. Therefore, to reach the same displacement imposed at the boundaries, a larger force is required in the circular case than in the rectangular case.

In Figure 6, center, the relative rigid displacement is in the direction orthogonal to the bisecting diameter and imposes a shear to the specimen. The resulting shear deformation pattern is similar to the one activated in extension (Figure 6, left), but with different orientations of the inner boundary layers. The comparison with the case of rectangular sheet leads to similar comments as above.

In Figure 6, right, the relative displacement of the two arcs is obtained by fixing one arc and by rotating the second one with respect the center of the circle. Remark that the partitioning of the specimen is similar as in the rectangular case but here the boundary layers invade the whole body.

6.3. ***Bias test on initially circular pantographic sheets with central holes.*** In the same body considered in the previous subsection, a square hole (of 14×14 cells) is now carved in its central part. The initial orientation of the hole relative to the fibers varies from zero (i.e., the sides of the square are along the fibers) to $\frac{1}{8}\pi$ and $\frac{1}{4}\pi$ (i.e., the edges of the square are along and orthogonal to the extension displacement). These different cases enable the investigation of the effect of the hole on the deformation pattern and on the onset of inner boundary layers.

One may expect that when a hole is carved in a subdomain corresponding to quasifloppy modes, its influence should be negligible since in both cases the hole or floppy modes deformation occurs with no energy expense. However, if a hole intersects the deformation boundary layers in which the energy would be localized

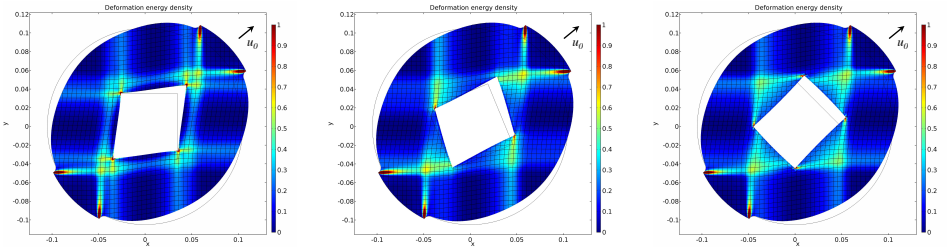

Figure 7. Equilibrium shapes for extension bias test of a circular sample with a squared hole: left, whose edges are oriented along fibers; center, rotated at an angle of $\frac{1}{8}\pi$; right, rotated at an angle of $\frac{1}{4}\pi$. The colors indicate the levels of stored energy density.

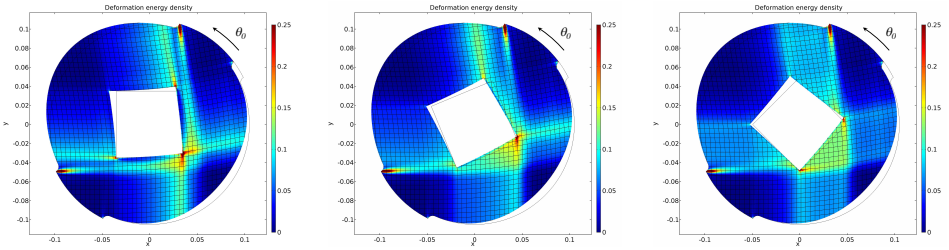

Figure 8. Equilibrium shapes for bending test of a circular sample with a squared hole: left, whose edges are oriented along fibers; center, rotated of an angle of $\pi/8$; right, rotated of an angle of $\frac{1}{4}\pi$. The colors indicate the levels of stored energy density.

in absence of a hole, then the energy distribution is necessarily modified and so does the deformation patterns.

This is what is observed in the simulations. The edges of the carved hole are such that when oriented along the fibers, the hole almost belongs to the central floppy mode subdomain that arises in the noncarved sheet, while when rotated, two corners of the hole may cross the boundary layers of the intact sheet. In extension tests presented in Figures 7, left and right, the intersection of the carved hole with the deformation boundary layers of the intact body is relatively small and the deformation patterns are weakly disturbed. This is not the case in Figure 7, center, where the hole cuts the material lines, i.e., fibers in which the energy would be concentrated in an intact body. As a consequence, the deformation response and the partitioning of the specimen change significantly. The same trends are observed for the bending test: weak perturbations arise in Figure 8, left, but large and dramatic change appears in Figure 8, center and right, respectively.

7. Conclusions

Pantographic sheets belong to the specific class of architectured materials whose mechanical behavior is characterized by:

- very high contrast of extensional and bending stiffness at microscopic level (see (35));
- very high contrasted gradients of displacement in the axial and transverse direction at the macrolevel (see (40));
- a microstructure which produces a discretely oriented, orthotropic material exhibiting an extreme anisotropy leading to the presence of two preferred material directions having very high extensional stiffness; this circumstance causes the onset of internal boundary layers where gradients of deformation may arise.

The standard (Cauchy or first gradient) continuum models were conceived under some implicit assumptions which do not allow for the description of all above listed extreme mechanical properties [dell'Isola et al. 2015a]. For this reason, it is needed to introduce, for pantographic sheets, a generalized continuum model by reconsidering, at the very beginning, the standard modeling procedure. Indeed a consistent model should allow for, in particular, the description of deformation gradient concentrations induced by imposed boundary displacements. To be driven in the construction of the most suitable model we use the asymptotic homogenization method extensively presented in [Boutin and Auriault 1993]. It allows for the rigorous construction of a description able to encompass all mentioned atypical properties.

Even if we limit ourselves to the case of linearized models in statics (and in the absence of body forces), we still get a nonstandard second gradient continuum model. Moreover, the advantage of used micro-macro upscaling procedure is that it allows us to determine firstly the atypical structure of the constitutive and balance equations and secondly all relative constitutive parameters (i.e., those specifying the first gradient and second gradient terms in deformation energy). This is done explicitly in terms of the microscopic properties of the elementary cells constituting the pantographic sheet. Furthermore, the presented micro-macro identification provides a design rule for pantographic bidimensional continua.

The main advances provided by this paper compared to some previous works on pantographic sheets lie in the three following points:

- The homogenization method leads to a clear and rigorous micro-macro identification procedure. Hence, the structure of the homogenized description and its parameters are explicitly deduced from the cell. This differs from the *a priori* variational approaches where a macroscopic description is proposed

but its applicability to specific microstructures can only be postulated. Besides, compared to direct numerical simulations at the microscale [dell'Isola et al. 2016b], the established model presents a great advantage, in terms of computational cost and also of in terms of physical understanding of the actual behavior.

- The description enables us to account for the low extensibility and the high bending deformability. It thus enables us to overcome the drawback of the studies that consider inextensible fibers [dell'Isola et al. 2016c].
- The physical insight of pantographic systems is improved by a simple interpretation of the macroscopic description: the tension in a fiber varies because of the shear forces transferred through the pivots by the orthogonal fibers. Even if the paper focuses on small deformations, this mechanism remains essentially the same (albeit complicated by the nonorthogonality of the fibers) at large deformation [dell'Isola et al. 2016d].

Note that we only consider small in-plane deformations. However, the same homogenization method can be extended to investigate buckling and out-plane deformation as discussed in [Giorgio et al. 2015; 2016].

The obtained models can be framed in the context of generalized continuum theories and immediately allows for the explicit determination of the deformation energy and related boundary conditions. The atypical features of the described continuum model for pantographic sheets are reflected by its atypical mathematical properties. That is:

- the PDEs determining the equilibrium configurations involve second and forth-order partial derivatives terms which may have a comparable order of magnitude; in the studied case of orthogonal fibers, the displacement fields along the fibers are governed by uncoupled PDEs;
- the deformation energy is not coercive in the standard sense. However, using specific boundary conditions, consistently established from the found expression for deformation energy, we establish the definite positiveness of the deformation energy functional, which simultaneously involves first- and second-order of displacement gradients; we conjecture that such formulated problems are well-posed.

The corresponding atypical physical properties of pantographic sheets consist in the following circumstances:

- the extensional forces along a fiber are balanced by the shear forces due to the bending of its transverse fibers (see (44), (45)),

- the balance of couples is separately valid for the two arrays of orthogonal fibers, so that the fiber rotation is proportional to the axial gradient of transverse displacement; see (46).

The numerical simulations which we have presented are aimed at illustrating the performances of the obtained model. Indeed, pantographic sheets show very peculiar deformation patterns exhibiting regions of concentrated deformation energy. In particular, when applied to rectangular specimen the model:

- it allows for the determination, already in the linear case, of the region where the deformation energy is localized without any further *a priori* assumptions;
- it shows that the diffusion patterns of deformation inside the specimen differ notably from those shown in first gradient material. In particular, they are canalized in a way determined by the material symmetry and boundary conditions, while their thickness is determined by the characteristic length specified by the competition between the first and second gradient stiffnesses;
- the described features are confirmed by considering a specimen of circular shape with rectangular holes.

All these features and predictions match at least qualitatively the experimental evidence, e.g., [dell'Isola et al. 2015b]. It then appears that the pantographic sheet is an archetypical-oriented material in which second gradient effect plays a crucial role and for which it is possible to get a close description of the underlying actual physical mechanism.

There are many worthy issues that may be investigated concerning the complex structure here analyzed:

- a linearized analysis of pantographic structures with nonorthogonal and uneven fibers (this case is also relevant as it may give a tangent model for large deformations) and the determination of some analytical solutions of found PDEs;
- the comparison of the presented theory with further experimental evidence for possible improvement in the idealized model;
- the exploration of the application of the model to the mechanics of fabrics, the analysis of the dissipation that can arise from the interaction of the fibers or from internal friction (see, e.g., [Nadler and Steigmann 2003]) and the extension to three-dimensional deformations;
- buckling phenomena which can produce wrinkling (see, e.g., [Giorgio et al. 2016; Rizzi and Varano 2011; Rizzi et al. 2013; Gabriele et al. 2012; Carassale and Piccardo 2010; Piccardo et al. 2015]) and damage detection and its evolution (see, e.g., [Yang et al. 2011; Misra and Singh 2013; Andreaus and Casini 2016; Placidi 2015; Placidi 2016]).

Finally, as future and more challenging lines develop, considering biological applications, it is conceivable that a morphoelastic pantographic continuum can be employed as a "smart" prosthesis (see, e.g., [McMahon et al. 2011]). In this context, it is possible also to equip the pantographic structure with transducers that can act both as sensors or actuators in order to induce some functional adaptation capabilities (see, e.g., [D'Annibale et al. 2015a; D'Annibale et al. 2015b; Andreaus and Porfiri 2007]).

Acknowledgements

Claude Boutin gratefully acknowledges the Università di Roma La Sapienza for a visiting grant. The authors thank Tomasz Lekszycki, Marek Pawlikowski and Roman Grygoruk for having made Figure 2 available.

References

[Abdiwi et al. 2013] F. Abdiwi, P. Harrison, and W. R. Yu, "Modelling the shear-tension coupling of woven engineering fabrics", *Adv. Materials Sci. Eng.* **2013** (2013), art. id. 786769, 9 pp.

[Alibert and Della Corte 2015] J.-J. Alibert and A. Della Corte, "Second-gradient continua as homogenized limit of pantographic microstructured plates: a rigorous proof", *Z. Angew. Math. Phys.* **66**:5 (2015), 2855–2870.

[Alibert et al. 2003] J.-J. Alibert, P. Seppecher, and F. dell'Isola, "Truss modular beams with deformation energy depending on higher displacement gradients", *Math. Mech. Solids* **8**:1 (2003), 51–73.

[Allaire 1992] G. Allaire, "Homogenization and two-scale convergence", *SIAM J. Math. Anal.* **23**:6 (1992), 1482–1518.

[Altenbach et al. 2011] H. Altenbach, V. A. Eremeyev, and L. P. Lebedev, "Micropolar shells as two-dimensional generalized continua models", pp. 23–55 in *Mechanics of generalized continua*, edited by H. Altenbach et al., Adv. Struct. Mater. **7**, Springer, Heidelberg, 2011.

[Andreaus and Casini 2016] U. Andreaus and P. Casini, "Identification of multiple open and fatigue cracks in beam-like structures using wavelets on deflection signals", *Contin. Mech. Thermodyn.* **28**:1–2 (2016), 361–378.

[Andreaus and Porfiri 2007] U. Andreaus and M. Porfiri, "Effect of electrical uncertainties on resonant piezoelectric shunting", *J. Intelligent Mat. Syst. Struct.* **18**:5 (2007), 477–485.

[Archimedes/Heath 1897] Archimedes, "On floating bodies", pp. 253–300 in *The works of Archimedes*, edited by T. L. Heath, Cambridge Univ. Press, 1897.

[Archimedes/Heath 1912] Archimedes, *The method of Archimedes, recently discovered by Heiberg: a supplement to the works of Archimedes, 1897*, edited by T. Heath, Cambridge Univ. Press, 1912.

[Auriault et al. 2009] J.-L. Auriault, C. Boutin, and C. Geindreau, *Homogenization of coupled phenomena in heterogenous media*, Wiley, Hoboken, NJ, 2009.

[Beirão da Veiga et al. 2008] L. Beirão da Veiga, J. Niiranen, and R. Stenberg, "A family of C^0 finite elements for Kirchhoff plates, II: Numerical results", *Comput. Methods Appl. Mech. Engrg.* **197**:21-24 (2008), 1850–1864.

[Bensoussan et al. 2011] A. Bensoussan, J.-L. Lions, and G. Papanicolaou, *Asymptotic analysis for periodic structures*, AMS, Providence, RI, 2011.

[Bîrsan et al. 2012] M. Bîrsan, H. Altenbach, T. Sadowski, V. A. Eremeyev, and D. Pietras, "Deformation analysis of functionally graded beams by the direct approach", *Compos. B: Engrg.* **43**:3 (2012), 1315–1328.

[Boutin and Auriault 1993] C. Boutin and J.-L. Auriault, "Rayleigh scattering in elastic composite materials", *Internat. J. Engrg. Sci.* **31**:12 (1993), 1669–1689.

[Boutin and Hans 2003] C. Boutin and S. Hans, "Homogenisation of periodic discrete medium: application to dynamics of framed structures", *Comp. Geotech.* **30**:4 (2003), 303–320.

[Boutin and Soubestre 2011] C. Boutin and J. Soubestre, "Generalized inner bending continua for linear fiber reinforced materials", *Int. J. Solids Structures* **48**:3–4 (2011), 517–534.

[Boutin et al. 2010] C. Boutin, S. Hans, and C. Chesnais, "Generalized beams and continua: dynamics of reticulated structures", pp. 131–141 in *Mechanics of generalized continua*, edited by G. A. Maugin and A. V. Metrikine, Adv. Mech. Math. **21**, Springer, New York, 2010.

[Caillerie 1984] D. Caillerie, "Thin elastic and periodic plates", *Math. Methods Appl. Sci.* **6**:2 (1984), 159–191.

[Camar-Eddine and Seppecher 2001] M. Camar-Eddine and P. Seppecher, "Non-local interactions resulting from the homogenization of a linear diffusive medium", *C. R. Acad. Sci. Paris Sér. I Math.* **332**:5 (2001), 485–490.

[Cao et al. 2008] J. Cao, R. Akkerman, P. Boisse, J. Chen, H. S. Cheng, E. F. de Graaf, J. L. Gorczyca, P. Harrison, G. Hivet, J. Launay, W. Lee, L. Liu, S. V. Lomov, A. Long, E. de Luycker, F. Morestin, J. Padvoiskis, X. Q. Peng, J. Sherwood, Tz. Stoilova, X. M. Tao, I. Verpoest, A. Willems, J. Wiggers, T. X. Yu, and B. Zhu, "Characterization of mechanical behavior of woven fabrics: experimental methods and benchmark results", *Compos. A: Appl. Sci. Manuf.* **39**:6 (2008), 1037–1053.

[Carassale and Piccardo 2010] L. Carassale and G. Piccardo, "Non-linear discrete models for the stochastic analysis of cables in turbulent wind", *Int. J. Non-Linear Mech.* **45**:3 (2010), 219–231.

[Carcaterra et al. 2015] A. Carcaterra, F. dell'Isola, R. Esposito, and M. Pulvirenti, "Macroscopic description of microscopically strongly inhomogeneous systems: a mathematical basis for the synthesis of higher gradients metamaterials", *Arch. Ration. Mech. Anal.* **218**:3 (2015), 1239–1262.

[Casal 1966] P. Casal, "Principes variationnels en fluide compressible et en magnétodynamique des fluides", *J. Méc., Paris* **5** (1966), 149–161.

[Cazzani et al. 2016a] A. Cazzani, M. Malagù, and E. Turco, "Isogeometric analysis of plane-curved beams", *Math. Mech. Solids* **21**:5 (2016), 562–577.

[Cazzani et al. 2016b] A. Cazzani, M. Malagù, E. Turco, and F. Stochino, "Constitutive models for strongly curved beams in the frame of isogeometric analysis", *Math. Mech. Solids* **21**:2 (2016), 182–209.

[Cecchi and Rizzi 2001] A. Cecchi and N. L. Rizzi, "Heterogeneous elastic solids: a mixed homogenization-rigidification technique", *Internat. J. Solids Structures* **38**:1 (2001), 29–36.

[Chesnais et al. 2015] C. Chesnais, C. Boutin, and S. Hans, "Wave propagation and non-local effects in periodic frame materials: generalized continuum mechanics", *Math. Mech. Solids* **20**:8 (2015), 929–958.

[d'Agostino et al. 2015] M. V. d'Agostino, I. Giorgio, L. Greco, A. Madeo, and P. Boisse, "Continuum and discrete models for structures including (quasi-)inexstensible elasticae with a view to the design and modeling of composite reinforcements", *Int. J. Solids Structures* **59** (2015), 1–17.

[D'Annibale et al. 2015a] F. D'Annibale, G. Rosi, and A. Luongo, "Linear stability of piezoelectric-controlled discrete mechanical systems under nonconservative positional forces", *Meccanica* **50**:3 (2015), 825–839.

[D'Annibale et al. 2015b] F. D'Annibale, G. Rosi, and A. Luongo, "On the failure of the 'similar piezoelectric control' in preventing loss of stability by nonconservative positional forces", *Z. Angew. Math. Phys.* **66**:4 (2015), 1949–1968.

[Del Vescovo and Giorgio 2014] D. Del Vescovo and I. Giorgio, "Dynamic problems for metamaterials: review of existing models and ideas for further research", *Internat. J. Engrg. Sci.* **80** (2014), 153–172.

[Della Corte et al. 2016] A. Della Corte, A. Battista, and F. dell'Isola, "Referential description of the evolution of a 2D swarm of robots interacting with the closer neighbors: perspectives of continuum modeling via higher gradient continua", *Int. J. Non-Linear Mech.* **80** (2016), 209–220.

[dell'Isola and Placidi 2011] F. dell'Isola and L. Placidi, "Variational principles are a powerful tool also for formulating field theories", pp. 1–15 in *Variational models and methods in solid and fluid mechanics*, edited by F. dell'Isola and S. Gavrilyuk, CISM Courses and Lect. **535**, Springer, Vienna, 2011.

[dell'Isola and Steigmann 2015] F. dell'Isola and D. Steigmann, "A two-dimensional gradient-elasticity theory for woven fabrics", *J. Elasticity* **118**:1 (2015), 113–125.

[dell'Isola et al. 2009] F. dell'Isola, A. Madeo, and P. Seppecher, "Boundary conditions at fluid-permeable interfaces in porous media: a variational approach", *Internat. J. Solids Structures* **46**:17 (2009), 3150–3164.

[dell'Isola et al. 2012] F. dell'Isola, P. Seppecher, and A. Madeo, "How contact interactions may depend on the shape of Cauchy cuts in *N*th gradient continua: approach '*à la* d'Alembert"', *Z. Angew. Math. Phys.* **63**:6 (2012), 1119–1141.

[dell'Isola et al. 2015a] F. dell'Isola, U. Andreaus, and L. Placidi, "At the origins and in the vanguard of peridynamics, non-local and higher-gradient continuum mechanics: an underestimated and still topical contribution of Gabrio Piola", *Math. Mech. Solids* **20**:8 (2015), 887–928.

[dell'Isola et al. 2015b] F. dell'Isola, T. Lekszycki, M. Pawlikowski, R. Grygoruk, and L. Greco, "Designing a light fabric metamaterial being highly macroscopically tough under directional extension: first experimental evidence", *Z. Angew. Math. Phys.* **66**:6 (2015), 3473–3498.

[dell'Isola et al. 2015c] F. dell'Isola, P. Seppecher, and A. Della Corte, "The postulations *à la* d'Alembert and *à la* Cauchy for higher gradient continuum theories are equivalent: a review of existing results", *Proc. A.* **471**:2183 (2015), art. id. 20150415, 25 pp.

[dell'Isola et al. 2016a] F. dell'Isola, A. Della Corte, and I. Giorgio, "Higher-gradient continua: the legacy of Piola, Mindlin, Sedov and Toupin and some future research perspectives", 2016. To appear in *Math. Mech. Solids*.

[dell'Isola et al. 2016b] F. dell'Isola, A. Della Corte, I. Giorgio, and D. Scerrato, "Pantographic 2D sheets: discussions of some numerical investigations and potential applications", *Int. J. Non-Linear Mech.* **80** (2016), 200–208.

[dell'Isola et al. 2016c] F. dell'Isola, A. Della Corte, L. Greco, and A. Luongo, "Plane bias extension test for a continuum with two inextensible families of fibres: a variational treatment with Lagrange multipliers and a perturbation design", *Int. J. Solids Structures* **81** (2016), 1–12.

[dell'Isola et al. 2016d] F. dell'Isola, I. Giorgio, M. Pawlikowski, and N. L. Rizzi, "Large deformations of planar extensible beams and pantographic lattices: heuristic homogenization, experimental and numerical examples of equilibrium", *Proc. Royal. Soc. A* **472**:2185 (2016), art. id. 20150790, 23 pp.

[dell'Isola et al. 2016e] F. dell'Isola, A. Madeo, and P. Seppecher, "Cauchy tetrahedron argument applied to higher contact interactions", *Arch. Ration. Mech. Anal.* **219**:3 (2016), 1305–1341.

[Dieudonné 1987] J. Dieudonné, *Pour l'honneur de l'esprit humain: les mathématiques aujourd'hui*, Librairie Hachette, Paris, 1987.

[Eremeyev 2016] V. A. Eremeyev, "On effective properties of materials at the nano- and microscales considering surface effects", *Acta Mech.* **227**:1 (2016), 29–42.

[Eremeyev and Lebedev 2011] V. A. Eremeyev and L. P. Lebedev, "Existence theorems in the linear theory of micropolar shells", *Z. Angew. Math. Mech.* **91**:6 (2011), 468–476.

[Federico and Grillo 2012] S. Federico and A. Grillo, "Elasticity and permeability of porous fibre-reinforced materials under large deformations", *Mech. Materials* **44** (2012), 58–71.

[Gabriele et al. 2012] S. Gabriele, N. Rizzi, and V. Varano, "On the imperfection sensitivity of thin-walled frames", pp. 1–17, Paper 15 in *Proceedings of the Eleventh International Conference on Computational Structures Technology*, edited by B. H. V. Topping, Civil-Comp Proceedings **99**, Civil-Comp Press, Slingshire, UK, 2012.

[Germain 1973] P. Germain, "The method of virtual power in continuum mechanics, II: Microstructure", *SIAM J. Appl. Math.* **25**:3 (1973), 556–575.

[Giorgio et al. 2015] I. Giorgio, R. Grygoruk, F. dell'Isola, and D. J. Steigmann, "Pattern formation in the three-dimensional deformations of fibered sheets", *Mech. Res. Comm.* **69** (2015), 164–171.

[Giorgio et al. 2016] I. Giorgio, A. Della Corte, F. dell'Isola, and D. J. Steigmann, "Buckling modes in pantographic lattices", *Comptes Rendus Méc.* **344**:7 (2016), 487–501.

[Gouin and Debieve 1986] H. Gouin and J.-F. Debieve, "Variational principle involving the stress tensor in elastodynamics", *Int. J. Eng. Sci.* **24**:7 (1986).

[Greco and Cuomo 2013] L. Greco and M. Cuomo, "B-spline interpolation of Kirchhoff–Love space rods", *Comput. Methods Appl. Mech. Engrg.* **256** (2013), 251–269.

[Greco and Cuomo 2014] L. Greco and M. Cuomo, "An implicit G^1 multi patch B-spline interpolation for Kirchhoff–Love space rod", *Comput. Methods Appl. Mech. Engrg.* **269** (2014), 173–197.

[Greco and Cuomo 2015] L. Greco and M. Cuomo, "Consistent tangent operator for an exact Kirchhoff rod model", *Contin. Mech. Thermodyn.* **27**:4 (2015), 861–877.

[Greco and Cuomo 2016] L. Greco and M. Cuomo, "An isogeometric implicit G^1 mixed finite element for Kirchhoff space rods", *Comput. Methods Appl. Mech. Engrg.* **298** (2016), 325–349.

[Grillo et al. 2015] A. Grillo, G. Wittum, A. Tomic, and S. Federico, "Remodelling in statistically oriented fibre-reinforced materials and biological tissues", *Math. Mech. Solids* **20**:9 (2015), 1107–1129.

[Hans and Boutin 2008] S. Hans and C. Boutin, "Dynamics of discrete framed structures: a unified homogenized description", *J. Mech. Materials Struct.* **3**:9 (2008), 1709–1739.

[Harrison 2016] P. Harrison, "Modelling the forming mechanics of engineering fabrics using a mutually constrained pantographic beam and membrane mesh", *Compos. A: Appl. Sci. Manuf.* **81** (2016), 145–157.

[Heath 1921a] Sir T. Heath, *A history of Greek mathematics, I: From Thales to Euclid*, Clarendon, Oxford, 1921.

[Heath 1921b] Sir T. Heath, *A history of Greek mathematics, II: From Aristarchus to Diophantus*, Clarendon, Oxford, 1921.

[Hero/Woodcroft 1851] B. Woodcroft (editor), *The pneumatics of Hero of Alexandria*, C. Whittingham, London, 1851.

[Launay et al. 2008] J. Launay, G. Hivet, A. V. Duong, and P. Boisse, "Experimental analysis of the influence of tensions on in plane shear behaviour of woven composite reinforcements", *Composites Sci. Tech.* **68**:2 (2008), 506–515.

[Lekszycki 1991] T. Lekszycki, "Application of variational methods in analysis and synthesis of viscoelastic continuous systems", *Mech. Struct. Machines* **19**:2 (1991), 163–192.

[Liew et al. 2000] J. Y. R. Liew, H. Chen, N. E. Shanmugam, and W. F. Chen, "Improved nonlinear plastic hinge analysis of space frame structures", *Engrg. Struct.* **22**:10 (2000), 1324–1338.

[Madeo et al. 2015] A. Madeo, A. Della Corte, L. Greco, and P. Neff, "Wave propagation in pantographic 2D lattices with internal discontinuities", *Proc. Estonian Acad. Sci.* **64**:3S (2015), 325–330.

[McMahon et al. 2011] J. McMahon, A. Goriely, and M. Tabor, "Nonlinear morphoelastic plates, II: Exodus to buckled states", *Math. Mech. Solids* **16**:8 (2011), 833–871.

[Melnik and Goriely 2013] A. V. Melnik and A. Goriely, "Dynamic fiber reorientation in a fiber-reinforced hyperelastic material", *Math. Mech. Solids* **18**:6 (2013), 634–648.

[Mindlin 1964] R. D. Mindlin, "Micro-structure in linear elasticity", *Arch. Rational Mech. Anal.* **16**:1 (1964), 51–78.

[Mindlin 1965] R. D. Mindlin, "Second gradient of strain and surface-tension in linear elasticity", *Int. J. Solids Structures* **1**:4 (1965), 417–438.

[Misra and Singh 2013] A. Misra and V. Singh, "Micromechanical model for viscoelastic materials undergoing damage", *Contin. Mech. Thermodyn.* **25**:2-4 (2013), 343–358.

[Nadler and Steigmann 2003] B. Nadler and D. J. Steigmann, "A model for frictional slip in woven fabrics", *C. R. Méc. Acad. Sci. Paris* **331**:12 (2003), 797–804.

[Németh and Kocsis 2014] R. K. Németh and A. Kocsis, "Bielastic web of links: a discrete model of Csonka's beam", *Int. J. Non-Linear Mech.* **63** (2014), 49–59.

[Nikopour and Selvadurai 2014] H. Nikopour and A. P. S. Selvadurai, "Concentrated loading of a fibre-reinforced composite plate: experimental and computational modeling of boundary fixity", *Compos. B: Engrg.* **60** (2014), 297–305.

[Noor et al. 1978] A. K. Noor, M. S. Anderson, and W. H. Greene, "Continuum models for beam- and platelike lattice structures", *AIAA J.* **16**:12 (1978), 1219–1228.

[Piccardo et al. 2015] G. Piccardo, L. C. Pagnini, and F. Tubino, "Some research perspectives in galloping phenomena: critical conditions and post-critical behavior", *Contin. Mech. Thermodyn.* **27**:1–2 (2015), 261–285.

[Pideri and Seppecher 1997] C. Pideri and P. Seppecher, "A second gradient material resulting from the homogenization of an heterogeneous linear elastic medium", *Contin. Mech. Thermodyn.* **9**:5 (1997), 241–257.

[Piola 2014] G. Piola, *The complete works of Gabrio Piola, I*, edited by F. dell'Isola et al., Advanced Structured Materials **38**, Springer, Cham, Switzerland, 2014.

[Pipkin 1980] A. C. Pipkin, "Some developments in the theory of inextensible networks", *Quart. Appl. Math.* **38**:3 (1980), 343–355.

[Pipkin 1981] A. C. Pipkin, "Plane traction problems for inextensible networks", *Quart. J. Mech. Appl. Math.* **34**:4 (1981), 415–429.

[Placidi 2015] L. Placidi, "A variational approach for a nonlinear 1-dimensional second gradient continuum damage model", *Contin. Mech. Thermodyn.* **27**:4–5 (2015), 623–638.

[Placidi 2016] L. Placidi, "A variational approach for a nonlinear one-dimensional damage-elasto-plastic second-gradient continuum model", *Contin. Mech. Thermodyn.* **28**:1–2 (2016), 119–137.

[Placidi et al. 2017] L. Placidi, U. Andreaus, and I. Giorgio, "Identification of two-dimensional pantographic structure via a linear D4 orthotropic second gradient elastic model", *J. Eng. Math.* **103**:1 (2017), 1–21.

[Rahali et al. 2015] Y. Rahali, I. Giorgio, J. F. Ganghoffer, and F. dell'Isola, "Homogenization *à la* Piola produces second gradient continuum models for linear pantographic lattices", *Internat. J. Engrg. Sci.* **97** (2015), 148–172.

[Rizzi and Varano 2011] N. L. Rizzi and V. Varano, "The effects of warping on the postbuckling behaviour of thin-walled structures", *Thin-Walled Struct.* **49**:9 (2011), 1091–1097.

[Rizzi et al. 2013] N. L. Rizzi, V. Varano, and S. Gabriele, "Initial postbuckling behavior of thin-walled frames under mode interaction", *Thin-Walled Struct.* **68** (2013), 124–134.

[Russo 2004] L. Russo, *The forgotten revolution: how science was born in 300 BC and why it had to be reborn*, Springer, Berlin, 2004.

[Seppecher et al. 2011] P. Seppecher, J.-J. Alibert, and F. dell'Isola, "Linear elastic trusses leading to continua with exotic mechanical interactions", *J. Phys: Conf. Series* **319**:1 (2011), art. id. 012018, 1–13.

[Soubestre and Boutin 2012] J. Soubestre and C. Boutin, "Non-local dynamic behavior of linear fiber reinforced materials", *Mech. Materials* **55** (2012), 16–32.

[Steigmann and dell'Isola 2015] D. J. Steigmann and F. dell'Isola, "Mechanical response of fabric sheets to three-dimensional bending, twisting, and stretching", *Acta Mech. Sin.* **31**:3 (2015), 373–382.

[Toupin 1964] R. A. Toupin, "Theories of elasticity with couple-stress", *Arch. Rational Mech. Anal.* **17**:2 (1964), 85–112.

[Turco and Aristodemo 1998] E. Turco and M. Aristodemo, "A three-dimensional B-spline boundary element", *Comput. Methods Appl. Mech. Eng.* **155**:1–2 (1998), 119–128.

[Yang et al. 2011] Y. Yang, W. Y. Ching, and A. Misra, "Higher-order continuum theory applied to fracture simulation of nanoscale intergranular glassy film", *J. Nanomech. Micromech.* **1**:2 (2011), 60–71.

Received 9 Mar 2016. Revised 26 Oct 2016. Accepted 11 Jan 2017.

CLAUDE BOUTIN: claude.boutin@entpe.fr
Département Génie Civil et Bâtiment - URA CNRS 1652, Ecole Nationale des Travaux Publics de l'Etat - Université de Lyon, rue Maurice Audin, 69518 Vaulx-en-Velin, France

FRANCESCO DELL'ISOLA: francesco.dellisola@uniroma1.it
Dept. di Ingegneria Strutturale e Geotecnica, Università di Roma "La Sapienza", Via Eudossiana 18, I-00184 Roma, Italy

IVAN GIORGIO: ivan.giorgio@uniroma1.it
Università di Roma "La Sapienza", Via Eudossiana 18, I-00184 Roma, Italy

LUCA PLACIDI: luca.placidi@uninettunouniversity.net
International Telematic University Uninettuno, C.so Vittorio Emanuele II, 39, I-00186 Roma, Italy